Volume 54
Number 15
7 August 2025
Pages 7019–7340

# Chem Soc Rev

Chemical Society Reviews

rsc.li/chem-soc-rev

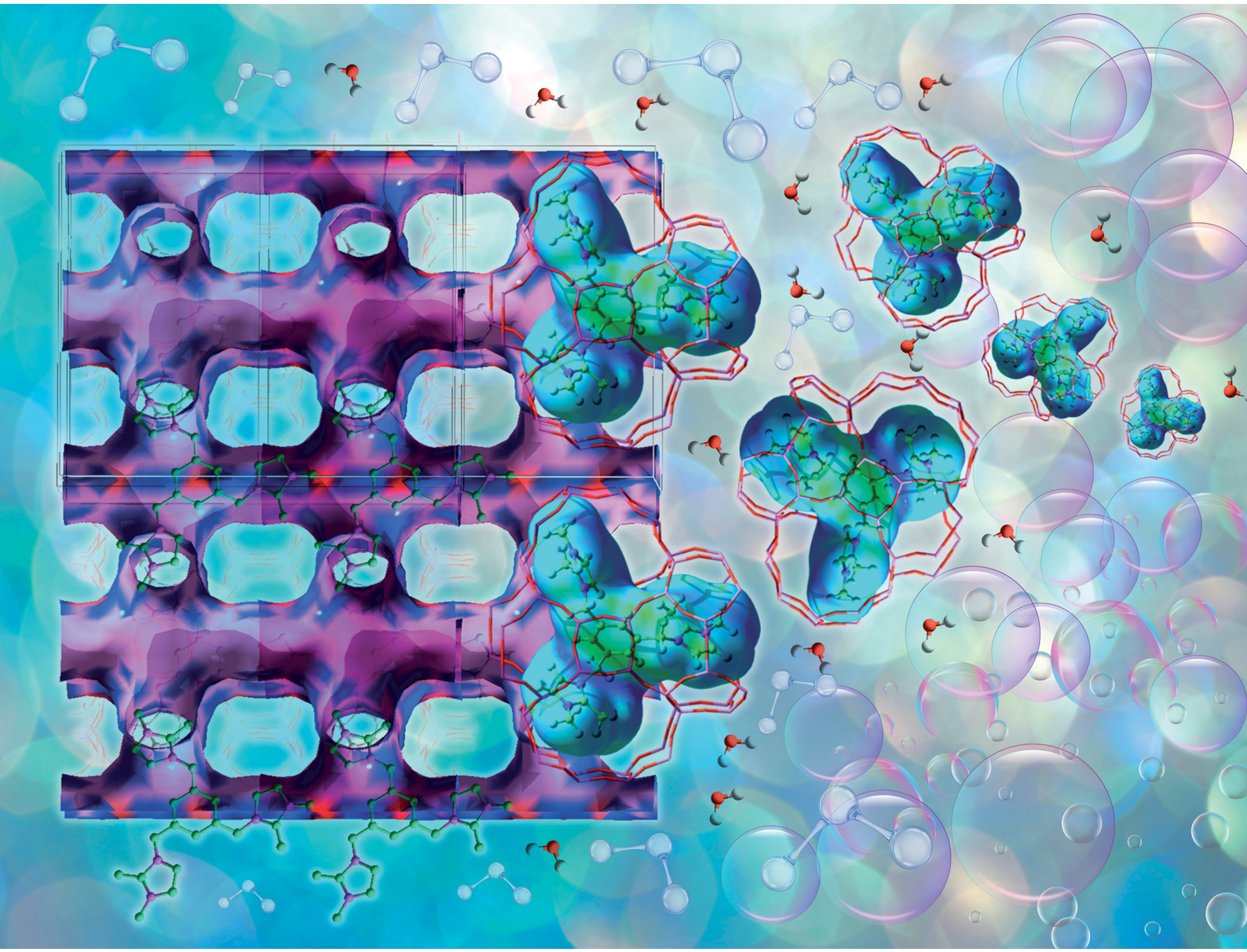

ISSN 0306-0012

ROYAL SOCIETY OF CHEMISTRY

**REVIEW ARTICLE**

German Sastre *et al.*

Computational insights on the role of structure-directing agents (SDAs) in the synthesis of zeolites

Chem Soc Rev

REVIEW ARTICLE

View Article Online
View Journal | View Issue



Cite this: *Chem. Soc. Rev.*, 2025, **54**, 7067

# Computational insights on the role of structure-directing agents (SDAs) in the synthesis of zeolites

Xiaomin Tang, [a] Omer F. Altundal, [b] Frits Daeyaert, [c] Zhiqiang Liu [d] and German Sastre *[b]

Most of the zeolites synthesised in the last 3 or 4 decades employ organic structure-directing agents (OSDAs) in their synthesis. The synthesis or test of new OSDAs is a major driving force in order to achieve the goal of synthesising a new zeolite. Despite this, predicting which zeolite phase will form when a specific OSDA is used remains a complex challenge. Moreover, even knowing the zeolite phase that will be obtained using a given OSDA, it is not easy to always rationalise or fully explain the result obtained. Computational simulations have occasionally been employed, and in a number of cases they are limited to calculate the van der Waals contribution between zeolite and the OSDA molecules (zeo–OSDA). Strongly negative values indicate an increasing viability of the synthesis, but it is only by comparison between competing zeolite phases that some insight can be gained, and this has been done in a limited number of cases. Other, less simple, approaches consider the total energy of the zeolite formed, of which the van der Waals zeo–OSDA contribution is not always the dominant contribution. These and other similar procedures need to be analysed and summarised in order to clarify the pros and cons of each approach. The recent advent of big data has allowed to construct databases that make it possible to analyse a large number of results. With the help of new descriptors and algorithms (some of them making use of artificial intelligence) further advances have been made. In spite of the large pool of data available, it becomes difficult to systematise and obtain general rules. A recent burst to this topic comes from the possibility to (at least partially) control the Al distributions by selecting appropriate OSDAs. These Al distributions influence the location and strength of Brønsted acid sites which in turn are directly responsible for the catalytic activity of the material.

Received 20th March 2025

DOI: 10.1039/d5cs00306g

rsc.li/chem-soc-rev



[a] *State Key Laboratory of Magnetic Resonance Spectroscopy and Imaging, National Center for Magnetic Resonance in Wuhan, Innovation Academy for Precision Measurement Science and Technology, Chinese Academy of Sciences, 430071 Wuhan, P. R. China*
[b] *Instituto de Tecnologia Quimica UPV/CSIC, Universidad Politecnica de Valencia, Valencia, 46022, Spain. E-mail: gsastre@itq.upv.es*
[c] *SynopsisDeNovoDesign, Beerse, 2340, Belgium*
[d] *Interdisciplinary Institute of NMR and Molecular Sciences, Hubei Province for Coal Conversion and New Carbon Materials, School of Chemistry and Chemical Engineering, Wuhan University of Science and Technology, Wuhan, 430081, P. R. China*

**Xiaomin Tang**

*Xiaomin Tang received her PhD in Physical Chemistry at the University of Chinese Academy of Sciences in 2021 under the supervision of Prof. Anmin Zheng. Following her doctoral studies, she continued her research as a Post-doctoral Fellow in Prof. Anmin Zheng's group, focusing on the framework aluminum distribution and catalytic reaction mechanism in zeolites by theoretical calculations.*

**Omer F. Altundal**

*Ömer Faruk Altundal received his MSc in Chemical and Biological Engineering from Koç University and completed his PhD in Sustainable Chemistry at Universitat Politècnica de València in 2025 under the supervision of German Sastre. His research focuses on molecular modelling of porous materials, with particular interests in the design of COFs (covalent organic frameworks) and zeolites for catalysis and separation applications.*

## 1. Introduction

With the title 'Hydrothermal Chemistry of the Silicates. Part IX. Nitrogenous Aluminosilicates', Barrer and Denny,[1] in 1961, introduced organic structure directing agents (OSDAs) into the synthesis of zeolites. This has been a breakthrough of far reaching impact and consequences. Before, the synthesis of zeolites had been structurally driven by the presence of inorganic cations, sited extra framework, which compensated the negative charge of the silico–aluminate.

Zeolites at the time were only known as aluminosilicates, mostly in the range of low Si/Al (between 1 and 5) and with relatively high densities. By 1980 the number of Zeolite Framework Type codes assigned to new zeolites synthesised using OSDAs was still as low as 5 (EAB, GIS, RUT, MEL, MFI), with, for instance, tetramethylammonium (TMA) and tetrabutylammonium (TBA) as OSDAs for TMA-E (EAB)[2] and ZSM-11 (MEL),[3] respectively. Hence it took a long time to realise the advantages of using OSDAs in the synthesis.

This contribution was not intended as an exhaustive review of computational work on the application of OSDAs in zeolite science. Rather, we wish to describe the progress of experimental knowledge and focus on how contributions from computational chemistry rationalise and eventually aid zeolite synthesis.

## 2. Early times, fundamental concepts, and way beyond

Unlike small inorganic cations whose location is only driven by electrostatics, organic cations bring into play short-range van der Waals (vdW) zeo–OSDA interactions and hence the idea of shape correspondence between OSDA and micropores appears.[4]

Cox and co-workers performed structure analysis on 160 OSDAs using force field simulations and provided a relatively quick and simple quantitative definition of the OSDA shape by employing inertial ellipsoids.[5] The inertial ellipsoids were defined by scaled inertial principal axes RX, RY, and RZ, which are inversely proportional to the corresponding principal moments. For instance, the cage-like pores of NON-type zeolites are templated by spherical or toroidal small molecules such as adamantanes and saturated ring compounds, and the NON-directing OSDAs therefore share principal moments of inertia that have similar values for each of the three components. The clustering of the data points depicting the principal moments of inertia for frameworks is indicative of the correlation between OSDA shape and resulting zeolite, which highlighted the potential importance of shape analysis as a strategy in OSDA design.

**Frits Daeyaert**

*Frits Daeyaert, PhD, has a background in computational drug design in the pharmaceutical industry. As visiting scientist at Rice University (Houston) he has developed and applied de novo design methods for the design of organic structure directing agents for the synthesis of zeolites. He is a co-recipient of the 2019 Breck award in Molecular Sieve Science for his contribution to the discovery of enantiomerically enriched STW zeolite.*

**Zhiqiang Liu**

*Zhiqiang Liu has been a professor at Wuhan University of Science and Technology since 2023. He received his PhD in Physical Chemistry at the University of Chinese Academy of Sciences with Prof. Anmin Zheng in 2018. His research focuses on the adsorption and diffusion mechanisms in zeolites using theoretical calculations.*

**German Sastre**

*German Sastre is Research Scientist at ITQ (Valencia). He made a postdoc at The Royal Institution of Great Britain with Sir Richard Catlow in 1995–1996. Since then, in ITQ, he employs computational chemistry methods to simulate synthesis of zeolites, catalytic and adsorption/diffusion processes, and physico-chemical properties of microporous materials (zeolites and metal–organic frameworks) and new families of materials such as Mxenes using big-data screening algorithms. He is, since 2013, member of the Structure Commission of the International Zeolite Association, and has served as scientific chair and member of research projects funding panels for FWO, NCN, GACR, EPSRC, FONCYT and FONDECYT.*

 

Usually, this is applied to pure silica zeolites, not only because of the simplicity of the calculations, without the need to guess the Al distribution, but also because in the absence of other structure directing effects such as Al, the role of zeo–OSDA van der Waals interactions ($E^{vdw}_{zeo-OSDA}$) becomes more important. Until Section 2.2, we will refer only to pure silica zeolites, without considering compensating anions such as hydroxide and fluoride. Although there are less than 50 computational publications associated with energy between OSDAs and pure silica zeolites before 2000, it gave satisfying results to a large extent and clarified the impact of OSDA on zeolite synthesis. Shen and Bell performed minimum-energy calculations and obtained the conformation of tetraalkylammonium cations (*i.e.*, TMA, tetraethylammonium (TEA), tetrapropylammonium (TPA) and TBA) occluded in ZSM-5 (MFI) and ZSM-11 (MEL) zeolites, as well as the stabilization energies of these OSDAs in zeolites.[6] It was found that both ZSM-5 and ZSM-11 zeolites could accommodate four TPA cations per unit cell and TPA was the most favourable OSDA for the stabilization of ZSM-5 zeolite, while four TBA cations preferred the stabilization of ZSM-11 over ZSM-5 zeolite due to the overcrowding of TBA cations in adjacent intersections of ZSM-5 zeolite.

A game changer review was published in 1992 by Davis and Lobo in which three degrees of increasing directing effects were distinguished for OSDAs: ''(i) space filling species, (ii) structure-directing agents, or (iii) templates. Organic species can fill the void space of high-silica zeolites. Since the surface of a forming high-silica crystal will be hydrophobic, the organic species will partition into these regions from the aqueous reaction mixture. By packing into the cages and channels, the organic species can increase the thermodynamic stability of the organic-framework composite over the stability (or more correctly metastability) of the framework alone. If structure-direction is occurring, then it should affect the nucleation process and ultimately the crystal structure that is formed. It is the question of the specificity of a particular structure to a particular organic that allows the distinction of structure-direction.''[7]

Also, the notion of hydrophilicity/hydrophobicity of the OSDAs was introduced by Kubota and coworkers and its importance in influencing the synthesis of high-silica zeolites was emphasised.[8] Goretsky *et al.*[9] further supported that OSDAs with similar size, but different hydrophilicity could impact nucleation and/or crystal growth of zeolite formation. The OSDA must be on the one hand polar enough to be dissolved in water but on the other hand must be hydrophobic enough to nucleate around the silica oligomers that will become the zeolite micropore. The phase transfer ratio of the iodide salts of positively charged OSDAs in water–chloroform mixtures has been proposed as a measure of the hydrophobicity of OSDAs and has been associated with C/N values. The simple parameter C/N ratio, in which 'C' stands for heavy uncharged atoms and 'N' stands for charged nitrogen atoms, has been found to describe the condition that OSDAs must fulfil in order to facilitate the nucleation and zeolite growth. The optimum range of C/N for quaternary ammonium cations is determined to be between 10 and 16,[8] whereas non-quaternary ammonium cations like imidazolium may have much lower values.[10]

As there was a clear correlation between the shape of OSDAs and zeolite channels,[11] ''shape'' was one criterion used to explain the specificity between OSDAs and zeolite micropores. Furthermore, with the advent of computational chemistry methods applied to study the effectiveness of OSDA–zeolite combinations, ''energy'' became a measure of the match between the OSDAs and the zeolite framework, and the OSDA–zeolite interaction energy has become the most commonly invoked concept to explain zeolite phase selectivity. The more negative the interaction energy, the better the OSDA for zeolite synthesis.

While the role of OSDAs in zeolite crystallization has been extensively investigated, their influence on nucleation and precursor stabilization remains an important yet less explored research. Jorge *et al.*[12] provided key computational insights into this early-stage process, showing that silica nanoparticles can form spontaneously in clear-solution zeolite synthesis before nucleation begins. Their Monte Carlo simulations revealed that these metastable nanoparticles form through silica condensation and hydrolysis and are stabilised by electrostatic interactions with TPA cations. They also found that higher pH leads to smaller, more stable nanoparticles, emphasizing how solution conditions and OSDA interactions shape the earliest stages of zeolite formation.

Building on this, Bertolazzo *et al.*[13] studied how these precursor nanoparticles transition into crystalline zeolites using classical nucleation theory combined with experimental data. Their findings show that zeolite formation does not follow a single-step process. Instead, it occurs through a spinodal-like mechanism, where many tiny zeolite crystals form and compete for growth within the amorphous precursor phase. Importantly, they found that polymorph selection happens after nucleation, during the later stages of crystal growth and coarsening, rather than being decided at the start. Their application of classical nucleation theory helped explain how energy barriers and precursor stability influence which structures emerge.

### 2.1 The simplification of using only van der Waals zeo–OSDA interactions

OSDAs are far from being selective molecules as can be seen from the widely known long list of zeolites that can be obtained with each OSDA. However, for strictly pure silica zeolites, when heteroatoms are not influencing the directing role, van der Waals interactions become significantly more pronounced. Ata *et al.*[14] investigated the strength of dispersion forces in various pure-silica zeolite–OSDA assemblies using DFT calculations and demonstrated that these forces are heavily dependent on the number of hydrogen atoms in the OSDA, being approximately proportional to this count. They found that, for optimal H–O contacts, the energy contribution of dispersion forces is approximately $-2$ kcal mol$^{-1}$ per H atom where vdW energy is maximised and OSDA fully acts as template. Moini *et al.*[15] highlighted the importance of vdW interactions by showing that diquaternary cations (*i.e.*, $(CH_3)_3N^+(CH_2)_{10}N^+(CH_3)_3$) could direct the synthesis of multiple zeolites, including ZSM-12,

ZSM-48, NU-87, and ZSM-5, across gels with varying Si/Al ratios. However, when using a pure silica gel, only the all-silica ZSM-48 was obtained. The reduced variety of products implies that $E_{zeo-OSDA}^{vdw}$ dominates the synthesis outcome, and its calculation helps greatly to predict which zeolite will be formed with a given OSDA. Through a combination of experiments and DFT calculations, Zicovich-Wilson demonstrated that the vdW interaction between the zeolite and OSDA played a crucial role in stabilizing ITW over TON when using 1,3,4-trimethylimidazolium as the OSDA in fluoride media. Notably, zeolite TON can *in situ* transform into the more porous and less stable (in calcined form) ITW under specific synthesis conditions, demonstrating that the structure-direction can revert the inherent stability trend observed in the absence of host–guest interactions.[16] Njo and co-workers studied the interaction of *N*,*N*-diethyl-3,5-dimethylpiperidinium (DDP) ions with MFI and MEL frameworks using force field simulations,[17] and showed that the DDP stabilised MEL better than MFI, which was in accordance with the fact that pure MEL could be synthesised using DDP as OSDA. Ma *et al.*[18] calculated the van der Waals stabilisation energy between MEL framework and 3,5-dimethylpyridine cations connecting with ethyl, propyl, and butyl groups (Et-DMPy, Pr-DMPy, and Bu-DMPy) using molecular simulations based on classical force fields. It was found that Bu-DMPy demonstrated the strongest stabilisation energy and this OSDA was successfully introduced into the synthesis of MEL structure.

Studies based on van der Waals zeo–OSDA energies often rationalise the excellent match between OSDA and micropores but fail to explain why a specific OSDA can give several zeolites. For instance, Stevens *et al.*[11] found that dibenzyldimethylammonium (DBDM) was able to produce ZSM-12 (MTW), ZSM-50 (EUO), or beta (BEA) zeolites by modifying the synthesis conditions. However, there was still a clear correlation between the shape of DBDM and each of the three different zeolite channels through a different packing arrangement for OSDAs. Overall, although $E_{zeo-OSDA}^{vdw}$ is a rough approximation, it has been, and still is, very successful in terms of accuracy and simplicity.

### 2.2 Beyond van der Waals zeo–OSDA interactions

It is, however, important to note that one of the main approximations in calculating zeo–OSDA interactions, many times overlooked in computational work in pure silica zeolites even nowadays, is that the positive charge of the OSDA must be compensated by anions, usually $OH^-$ and often also $F^-$. The former leads to the introduction of structural defects (siloxy and silanol groups, $SiO^-$ and SiOH), and the latter leads to frameworks with a very small number of defects in which the $F^-$ anions are occluded in small cavities. Finally, the total energy ($E_{zeo} + E_{OSDA} + E_{zeo-OSDA}^{vdw} + E_{zeo-OSDA}^{Coulomb}$), which accounts for the intrinsic stability of both the zeolite and OSDA, along with their van der Waals and Coulombic interactions, rather than only $E_{zeo-OSDA}^{vdw}$ should be employed to characterise the stability, and this allows the introduction in the thermodynamic equations of the aluminosilicate composition in a natural way. Together with hydroxide and fluoride, aluminium is the third 'anion' that can compensate for the (usual) positive charge of the OSDA.

A recent study by Zones and coworkers indicates that although zeolite phase selectivity correlates, in general, with zeo–OSDA vdW interaction energy, it is important to note that inter-zeolite comparisons of interaction energies for a given OSDA are not straightforward since the zeolite host framework density, among other factors, also plays an important role.[19] As a result, vdW interaction energy normalised either by the number of T atoms or by the number of OSDA molecules per unit cell is not enough, especially when evaluating lower *vs.* higher framework density zeolite phases. In the competition between SSZ-43 (target zeolite), SSZ-31 (*STO) and SSZ-35 (STF), 14 OSDAs were evaluated using force field simulations. In only one case (OSDA-6) in which SSZ-43 was the product obtained, the zeo–OSDA vdW interaction energy was lowest for SSZ-43.[19] However, the strategy to design new OSDAs with as low as possible SSZ-43-OSDA vdW interaction energy was successful and SSZ-43 was obtained with two new diquaternary ammonium cations in the Si/Al interval between 25 and 150.

In a similar study based on force field calculations of vdW energies, the lower stabilization energy of *N*,*N*-diethyl-5,8-dimethylazonium bicyclo[3.2.2]nonane in CHA compared to SFW did not explain why SFW was obtained experimentally, indicating that ''comparisons between structure types are invalid''.[20] The same happens with another three OSDAs that are used to synthesise SFW, whose zeo–OSDA vdW stabilisation energy is lower for CHA. This suggests again that other descriptors such as 'total energy' (containing zeolite stability and other terms apart from vdW) and 'synthesis energy' (containing not only 'total energy' but also the energy of the gel composition reactants), may give a more complete energetic prediction than vdW zeo–OSDA interaction energy alone. For example, Shi *et al.*[21] calculated stabilisation energies between a set of 21 successful and unsuccessful OSDAs and all-silica STW to understand the templating activity of a set of imidazolium and pyrazolium OSDAs towards STW zeolite. The energy calculations consisted of DFT optimization of the OSDAs and simulated annealing molecular dynamics simulations using combined van der Waals and Coulomb energies. It was found that the successful OSDAs exhibited stronger host–guest interactions than the unsuccessful ones. In addition, it was observed that all successful OSDAs have more negative charge concentrated on the nitrogen atoms, as well as a smaller dipole moment. The results were used to design additional molecules as OSDAs directed towards STW, showing the utility of advanced energetic descriptors in rational OSDA design. Later, Shi *et al.*[22] aimed to design a cost-effective OSDA for the synthesis of MSE zeolite, addressing the high production costs associated with traditional OSDAs. They developed three potential OSDAs inspired by the conventional *N*,*N*,*N*′,*N*′-tetraethyl-exo-dicyclo[2.2.2]oct-7-ene-2,3:5,6-dipyrrolidinium (TEBOP), which is widely used in MSE synthesis. Among these, dispiro-[piperidine-1,2′-(1′,2′,3′,5′,6′,7′-hexahydrobenzo[1,2-*c*:4,5-*c*′]dipyrrolium)-6′,1′′-piperidine] (BPIP) stood out due to having the lowest stabilization energy (vdW + Coulomb) within the MSE framework, as calculated by force field simulations. This significant stabilization enabled BPIP to act as an efficient OSDA, successfully synthesizing MSE zeolites with high crystallinity.

 

Recently, Gong *et al.*[23] investigated the binding energies and OSDA deformation energies of 19 experimentally reported OSDAs and 62 OSDAs that were derivatives of the experimental OSDAs within AFX zeolite, using a combination of molecular mechanics and molecular dynamics simulations. Their results showed that the 19 experimentally reported OSDAs had more negative binding energies ($<12$ kJ mol$^{-1}$ per Si) and smaller deformation energies ($<60$ kJ mol$^{-1}$), validating their computational approach. Finally, they reported 16 OSDAs among the 62 derived OSDAs which have comparable binding energies with the experimental OSDAs and low OSDA deformation energies, suggesting that these OSDA can be used in the synthesis of AFX.

Fig. 1 shows different energetic descriptors used in computational studies to determine the relative stability of zeo–OSDA complexes in the order of increasing accuracy ($E_{vdw} \rightarrow E_{tot} \rightarrow E_{syn}$). Although synthesis energy ($E_{syn}$) accounts for additional thermodynamic contributions compared to vdW and total energy calculations, it remains an approximation and has several inherent limitations. One major limitation is the omission of solvation effects. In real synthesis conditions, charged OSDAs and fluoride anions interact with surrounding water molecules, but this interaction is not explicitly included in the synthesis energy calculations. Instead, OSDAs are treated as if they transition directly from the gas state to the zeolite. Additionally, synthesis energy does not fully capture kinetic factors that govern zeolite crystallization. While it ranks competing phases based on thermodynamic stability, it does not account for differences in nucleation barriers, which can significantly impact which zeolite phase is actually formed. On the other hand, it does explicitly consider Al distribution effects as these are included in the total energy of the zeolite–OSDA system, which is calculated for a statistically significant number of Al distributions, with the lowest-energy configurations selected as final representatives. Despite these limitations, synthesis energy provides a more complete framework than van der Waals or total energy calculations alone. Through this incorporation of additional thermodynamic terms, it gives a better estimation of competing zeolite phases with respect to previous approaches. Some of the limitations described above can be implemented in the next future for further refinement.

Two cases with two different OSDAs and zeolites are represented in the figure. In the first case (red lines in Fig. 1), $OSDA_1$ has a more favourable zeo–OSDA vdW energy with $zeo_1$ than with $zeo_2$. However, since zeolites have different intrinsic energies, which are inversely proportional to their framework densities,[24] as represented in the inset figure, the order of energies changes for the total energies of the zeo–OSDA complex, and $zeo_2$ becomes more favourable. Finally, the 'synthesis energies' ($E_{syn}$) of the zeo–OSDA pairs, a recently defined energetic descriptor that accounts for the energies of all components in the synthesis equation,[25] were in agreement with the result using total energies as $zeo_2$ was again the predicted outcome of the synthesis. An example of the first case (red lines in Fig. 1) is present in the study by Altundal *et al.*,[25] where MRE, the denser zeolite, is the experimentally synthesised zeolite using OSDA7 (hexamethonium) in pure-silica gel under $OH^-$ media, and this is supported by both the total energy and synthesis energy.

However, the zeo–OSDA vdW energy is actually in favour of EUO, the less dense zeolite. The second case (blue lines in Fig. 1) represents an OSDA for which the zeo–OSDA vdW energy

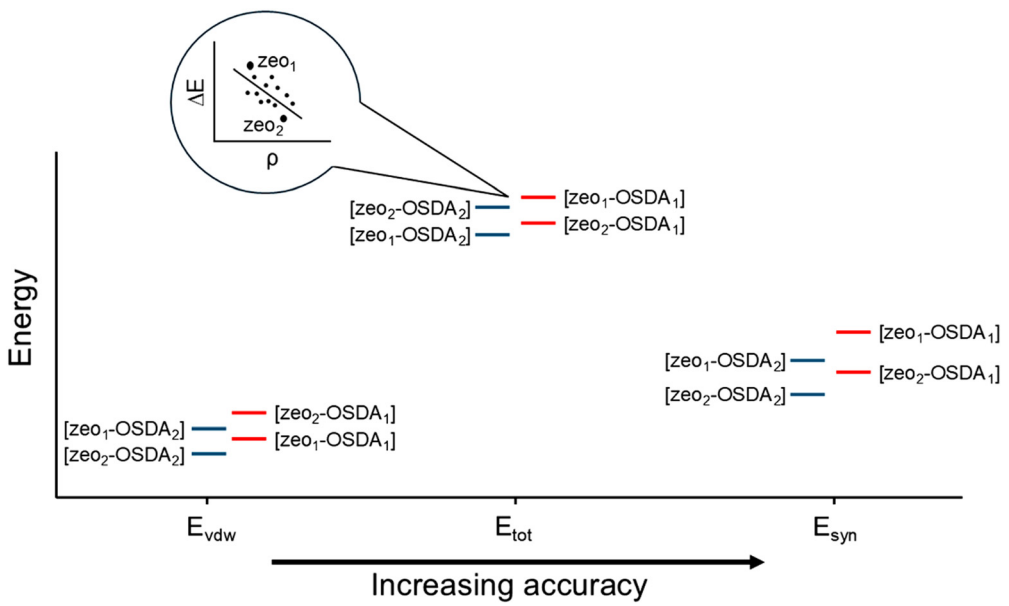


Fig. 1 Energetic descriptors used in computational studies to assess the stability of zeo–OSDA pairs in order of increasing accuracy ($E_{vdw} \rightarrow E_{tot} \rightarrow E_{syn}$). The generic examples illustrate how the relative stability of $zeo_1$ and $zeo_2$ may change depending on the OSDA employed in the synthesis. Also, the assessment of stability may be more or less accurate depending on the descriptor employed. The inset figure illustrates the relation between framework energy and density.[20]

is more favourable for $zeo_2$ instead of $zeo_1$. This case is seen in the work by Sastre *et al.*,[26] as the zeo–OSDA vdW interactions of EU-1 (EUO) and β zeolite (BEA) are stronger than that of ZSM-11 (MEL) when OSDA1 (*N*-cyclohexyl-*N*-methyl-pyrrolidinium) is used. Nevertheless, when OSDA2 (*N*-cyclohexyl-*N*-butyl-pyrrolidinium) is used in the synthesis, due to the large size of the cation, the OSDA is strained in the channels of EUO and BEA, and zeo–OSDA vdW energy of MEL becomes the most favourable. When the total and synthesis energies in the second case are considered, we see that the order of zeolite stabilities are different for both descriptors. In the paper of Altundal *et al.*,[25] a similar case is present with OSDA3 (1,1,3,5-tetramethylpiperidinium), where AEI and CHA have more favourable total energies than MTW in pure-silica $F^-$ media synthesis. However, according to the synthesis energies, MTW is predicted as the synthesis product, which fully agrees with the experimental studies. An additional case to show the insufficiency of vdW energies in determining phase selectivity appears for the interactions of 6,10-dimethyl-5-azoniaspiro[4.5]decane with STF and *STO zeolites. According to the study of Schwalbe-Koda *et al.*,[27] the vdW zeo–OSDA energy favours the formation of STF, which is the experimental zeolite phase obtained in fluoride media. However, the vdW energy is insufficient to explain the formation of *STO in hydroxide media, emphasising the need of a better descriptor to predict the phase selectivity. When using total energy as a descriptor, Leon and Sastre were able to predict the formation of STF in fluoride media and *STO in hydroxide media.[28] Overall, these cases highlight the importance of using energetic descriptors that account for all aspects of zeolite synthesis in comparing relative zeolite stability.

## 3. Role of aluminium as structure directing agent

Zeolite frameworks accommodate Al in each crystallographic position with different energetic stability, depending on geometrical and topological factors.[29] Different stabilities of T sites influence Al siting, which in turn determines the overall Al distribution within the framework. Al siting refers to the crystallographic position occupied by each Al atom, whilst Al distribution refers to each unique sequence of Al atoms substituted in the unit cell.[30] However, an additional driving force is the electrostatic interaction between Al and the positive charge of the OSDA, which tends to be dominant.

A strong relation between the position of aluminium and the structure directing agent was first suggested by Shantz and coworkers in 1999 indicating that an OSDA tends to reorientate its positive charge as close as possible to framework aluminium.[31] This suggests that the framework aluminium is directly associated with the charge centre of the OSDA.

In 2001,[32] it was explained how Al is preferentially located in the T4 position of ZSM-18 when using trispyrrolidinium cation as OSDA. This is not due to crystallographic but rather to electrostatic stability since T4 is closer to the quaternary ammonium centres where most of the positive charge is located. In fact, T4, within 3-rings, is the most disfavoured crystallographic location for Al. Shortly after, the same group was able to generate an Al and Brønsted site distribution for ITQ-7 in good agreement with infrared data by calculating the most stable Al distribution with data of the OSDA (1,3,3-trimethyl-6-azonium-tricyclo[3.2.1.$4^{6,6}$]dodecanehydroxide) location and charge distribution, as well as energetic stability of the corresponding Brønsted sites.[33]

With the advent of new experimental techniques to determine the Al distribution in *ca.* 2009, a new push appeared on this topic and the number of studies increased again, also initially focused on calcined zeolites, hence without trying to link the Al location with the OSDA employed in the synthesis.[34] For instance, Lu *et al.*[35] investigated the Al siting in MOR zeolite across various Si/Al ratios using a combined experimental and computational approach. After analysing the IR spectra of acetonitrile adsorbed in the zeolite channels, they realised that all MOR structures, regardless of Si/Al ratio, have the IR band that is assigned to the acidic OH groups in the side pockets ($T_3$ site). The stabilisation energies determined by DFT calculations, using zeolite models without the OSDA, showed that Al occupies the T sites in the order of preference $T_3 > T_4 > T_1 > T_2$, hence supporting that Al in the side pockets ($T_3$) is the most populated site, in agreement with the acetonitrile adsorption experiments. Similarly, Sklenak *et al.*[36] used a combined approach to elucidate Al siting in ZSM-5 zeolites with Si/Al ratios from 14 to 45. By comparing $^{27}$Al MQ MAS NMR spectroscopy data with chemical shifts calculated *via* QM/MM simulations, where Al atoms were modelled at distinct T sites, they identified specific occupied T sites in ZSM-5 samples and observed that siting of Al is considerably influenced by synthesis conditions. Furthermore, Dědeček *et al.*[37] presented the technique of cobalt titration to detect Al pairs, which nowadays is being widely used. Using this technique, Sazama *et al.*[38] explored how aluminium distribution in ZSM-5 impacts the catalytic cracking of 1-butene. Their results showed that Al distribution significantly affects reaction pathways for olefin transformation, with distributions featuring distant Al atoms promoting butene and octene cracking.

While the role of OSDA driving the Al distribution was soon recognised, at the time nothing was suggested on whether the presence of Al contributes to one or another zeolite phase to be formed. For many years a large number of computational studies focused on calculations of the stability of Al distributions on calcined zeolites, containing Brønsted sites, hence without considering the role of OSDA. Muraoka *et al.*[39] calculated the framework energies of 209 zeolite topologies with a wide range of Al contents (Si/Al = 1– $\infty$) using molecular simulations. Results indicated that Al prefers certain T sites in the structures, and the preferential siting of Al in certain T sites designates the feasible Al distributions and chemical compositions of a zeolite framework. Matsuoka *et al.*[40] analysed the preferential Al sites of 12 structures, which were carefully selected from a database of 900 000 hypothetical structures, by combining forcefield and DFT calculations. After introducing an Al atom in each distinct T site of these 12 structures,

 

generating a Brønsted site, they compared the acid strengths of these structures with those of well-known zeolites (FAU, BEA, and MFI) and found that 6 of the 12 structures exhibit significantly stronger acidity.

Finally, the role of OSDA was included in trying not only to find but also to justify, and even to partially design, the Al distribution in the zeolite, and in particular, how different OSDAs employed to synthesise a given zeolite were capable of generating very different Al distributions, with subsequent implications in catalysis. Di Iorio and Gounder investigated the effect of cationic charge density on the Al distribution of SSZ-13 (CHA) by changing the ratio of organic (*N*,*N*,*N*-trimethyl-1-adamantylammonium, $TMAda^+$) and inorganic ($Na^+$) structure-directing agents in the synthesis gel while keeping all other variables constant.[41] Using cobalt titration to identify Al proximity, they demonstrated that SSZ-13 synthesised exclusively with $TMAda^+$ cations does not contain any paired Al sites. However, introducing $Na^+$ into the synthesis gel caused a linear increase in the number of paired Al sites, reaching a maximum at a $Na^+/TMAda^+$ ratio of 1. Expanding on this approach, Gounder and coworkers investigated the aluminium siting in MFI zeolites in the presence of various OSDAs and $Na^+$ cations, incorporating computational methods alongside experiments.[42] DFT calculations, performed by incorporating one TPA cation and one Al atom at a random site in the MFI framework, revealed that the distance between the charge centre of the TPA cation and the Al atom has an inverse relationship with the stability of the MFI structure, showing the influence of electrostatic interactions on the siting of Al within the framework. Simulations with two TPA cations and two Al atoms in the unit cell illustrated that Al atoms can be paired with each other (within $\sim$5 Å) and still be close to TPA cation (within $\sim$7 Å), which is then validated by the $Co^{2+}$ titration experiments. When $Na^+$ cations were introduced to the synthesis, the number of paired Al atoms increased, similarly to the CHA case. Finally, using charge neutral OSDAs together with $Na^+$ cations decreased the Al content and the number of Al pairs in the MFI zeolite compared to the ones synthesised with TPA, suggesting that charge-neutral molecules can be utilised to direct the synthesis to frameworks with isolated Al sites. Recently, Gao *et al.*[43] explored the influence of OSDA charge distribution on Al siting in CHA through DFT calculations, using the $TMAda^+$ cation and four of its isomers where the charge centre ($N^+$) is moved to another location. They performed more than 1000 calculations for each OSDA considering various OSDA orientations and Al distributions and found that OSDAs which have a more accessible charge centre lead to a smaller Al–N distance which favours closer Al–Al distances. For example, one of the OSDAs with most accessible charge centres, 3-(*tert*-butyl)-1-azaadamantan-1-ium, favoured the formation of Al pairs in the 8-rings of CHA structure.

Román-Leshkov *et al.*[44] were able to control the Al distribution in ferrierite by selecting specific OSDAs: hexamethyleneimine, which preferentially promotes acid-site formation in 10-rings, and pyrrolidine, which favours Al incorporation into 8-rings. Muraoka *et al.*[45] synthesised IFR zeolites with controlled framework Al siting at different T sites and showed that OSDAs could alter the energetically favourable Al location by theoretical calculation and $^{27}Al$ MAS NMR. Biligetu *et al.*[46] synthesised ZSM-5 zeolite with various alcohols and found the Al atoms in the ZSM-5 synthesised with bulky and branched-chain alcohols (*e.g.*, trimethylolethane) in combination with $Na^+$ cations, were preferentially located in straight and/or sinusoidal channels, which was different from the location at the channel intersections using TPA cation as OSDA. Moreover, Wang and co-workers found that the distribution of Al atoms in the framework is a key factor in affecting the catalytic mechanism and further product selectivity.[47]

## 4. Role of fluoride as structure directing agent

The fluoride route was introduced initially by Flanigen and Patton,[48] later by Guth, Kessler, and Patarin,[49] and more recently by Camblor and coworkers, who have been able to synthesise a large number of new zeolites (ITE, IFR, STF, ISV, ITW, ITH, STT) as pure silica using this route.[50] Similarly to Al, fluoride was not initially recognised as SDA but rather only as a mineralizing agent whose role was to activate the formation and breaking of Si(Al)–O bonds. As opposed to the hydroxide route that works at high pH (typically above 11), the presence of fluoride allows the crystallisation at nearly neutral pH and increases the solubility of silica due to the formation of hexafluoro complexes, but the corresponding hexafluoroaluminates are less soluble.

The fluoride route has been proven to be very well suited for synthesising pure silica or very high silica materials, which in highly basic media lead to frameworks with a considerable number of connectivity defects, $SiO^-\cdots HOSi$ groups, which are the only anions capable of compensating the positive charge of the OSDA. The presence of $F^-$ allows to drastically reduce the number of such defects, leading to larger and more perfect crystals, with fewer defects, and also to new zeolite phases. The larger size of the crystals is probably due to a smaller nucleation rate, since supersaturation is presumably smaller in fluoride than in alkaline media. Using fluoride, it has not only been possible to obtain new pure silica zeolites such as ITQ-13 (ITH),[51] ITQ-12 (ITW),[52] ITQ-7 (ISV),[53] and ITQ-9 (STF),[54] but also new aluminosilicates such as ITQ-32 (IHW),[55] ITQ-39,[56] ITQ-10, and ITQ-27 (IWV),[57] new silico-germanates such as HPM-16 (–HOS),[58] ITQ-53 (–IFT),[59] and SU-32 (STW),[60] and new germanate zeolites such as IM-10 (UOZ),[61] FOS-5 (BEC),[62] ASU-7 (ASV), and ASU-9 (AST).[63]

Of these, ITH, ITW, ISV, AST, ITQ-10,[64] BEC, IWV, –IFT, –HOS, STW, UOZ, and ASV contain double four rings (D4Rs), the most common small cavity appearing in fluoride media, although many other small cavities, such as, among others, *sod*, *bea*, *rth*, *non*, $[4^35^4]$ (*t-bet*, STT, BEA), $[5^4]$ (*t-tes*, *mor*, FER), $[4^66^2]$ (*t-hpr*, *d6r*, CHA), $[4^35^26^2]$ (*t-wwf*, IFR) are also favourable to stabilise the fluoride anion inside.[50,65] It has been suggested

that fluoride stabilises 4-rings and, to a lesser extent, 5-rings and 6-rings. $^{19}$F NMR spectra allowed the characterisation of the type of small cavity in which fluoride is located.[66] It seems that the role of fluoride as SDA is mainly due to the stabilisation of zeolites containing specific small cavities. Additionally, pure silica zeolites containing D4R with AST, ISV, ITW, and ITH topologies have so far hardly (or never) been prepared without the use of fluoride, once again suggesting the strong structure directing and stabilising effect of the $F^-$ ion towards this secondary building block. Moreover, as suggested by Zicovich-Wilson *et al.*, fluoride reduces the covalent character of the Si–O bond, making it less directional and more flexible. This increased flexibility enables the formation of D4R structures that would otherwise be too strained to form in pure silica frameworks.[16,67] With the presence of fluoride, a computational study suggested that the electrostatic interactions of the [OSDA–F] subsystem (meaning OSDA–OSDA, OSDA–F, F–F), excluding the zeolite framework, plays a structure directing role. For silica IFR, ITH, IWR, STF, and STT structures containing fluoride, several fluoride locations were tested, with the experimental one giving the lowest electrostatic [OSDA–F] energy.[68]

## 5. Structure direction by the water/Si ratio in the presence of fluoride

It was discovered by Villaescusa and Camblor that,[69] in the presence of fluoride and with silica gels, the water/Si ratio plays a crucial role in the zeolite phase obtained. The so-called Villaescusa rule is that: the lower water/Si, the lower the density of the zeolite formed. Hence, going from the original recipe of water/Si *ca.* 15, to lower values, new zeolites were synthesised. For instance, the use of elongated bulky diquats with an approximately linear shape (such as $M_8BQ^{2+}$, $M_6BQ^{2+}$, *p*-$BBQ^{2+}$, $M_{10}BTM^{2+}$) as OSDAs could lead to the formation of both pure silica Beta and MTW zeolites. The water/Si ratio was able to regulate the phase selectivity of these OSDAs such that the less dense Beta with framework density (FD) of 15.6 T/1000 Å$^3$ was obtained at a lower water content (*e.g.*, water/Si = 7.5), while the denser MTW (FD is 18.2 T/1000 Å$^3$ in IZA website[70] while 19.4 T/1000 Å$^3$ according to ref. 69) was crystallised at a higher water/Si ratio of 15.0. The rule, originally discovered for silica zeolites, is also valid for aluminosilicates.[69] It is worth noting that the FD (T/1000 Å$^3$) values reported in the IZA database are derived from geometric DLS (distance least squares) refinement,[71] which may not always align with empirical data obtained from direct structure solutions. However, this approximation provides a reasonable level of accuracy. Therefore, unless otherwise specified, FD values in this work refer to those from the IZA database to maintain consistency.

The rule can be rationalised by considering that if the water/Si ratio decreases, the fluoride concentration increases, leading also to a larger concentration of OSDA, whose accommodation requires more open microporous space and hence lowers zeolite density. For example, the synthesis of chabazite (CHA) with FD, according to IZA, equal to 15.1 T/1000 Å$^3$ (FD is 15.4 T/1000 Å$^3$ according to ref. 69) using $TMAda^+$ as OSDA at 150 °C was heavily dependent on a very low water/Si ratio of 3.0 in the reaction mixture. The increase of water/Si to 5.8 produced mixed phases of chabazite and SSZ-23 (STT), and the amount of SSZ-23 increased with the heating time, the further increase of water/Si to 7.5 or 10 formed the only SSZ-23 phase, demonstrating that it favoured the denser SSZ-23 with FD of 17.0 T/1000 Å$^3$ at higher degrees of dilution.

The only reported exception is the crystallisation of STF (FD = 16.9 T/1000 Å$^3$) at lower water/silica ratios than ITE (FD = 15.7 T/1000 Å$^3$), although both zeolites occlude the same concentration of guests (2 OSDA/32Si) and have the same micropore volume in their calcined state (0.21 cm$^3$ g$^{-1}$).[72]

Whether this rule applies or not after addition of aluminium in the presence of fluoride is an interesting issue. Under these circumstances, both fluoride and aluminium compete as 'negative' ions that counterbalance the positive charge of the OSDA, and this has been studied for the synthesis of ITQ-4 (IFR) in aluminosilicate and fluoride media.[73] For a standard (*ca.* 15) water/silica ratio, in the presence of fluoride, when the Al content surpasses the OSDA content of the zeolite initially formed (ITQ-4), another less dense phase (beta) appears that can occlude a larger amount of OSDAs. As aluminium is introduced into the material, the amount of fluoride decreases, indicating a preference of aluminium over fluoride as 'anion' that compensates the positive charge of the OSDA. This has been justified in recent computational work in terms of 'synthesis energies'.[25,74] The phase selectivity change induced by an increasing aluminium content is the same as that induced by decreasing the water content. In more concentrated gels, with water/Si ratios between 3.5–7.5, the threshold Al content, Al/(Si + Al), for which the less dense (beta) phase appears (0.02) is lower than in the previous case (0.06) of more diluted gels, showing a more marked effect of the rule, as expected.[73]

The simulation of the effect of water/Si remains a difficult problem for computational chemistry since, among other reasons, the amount of water does not numerically affect the thermodynamic equations of the synthesis in a straightforward way. This is a very interesting challenge for future studies.

## 6. The excess fluoride approach

As explained in the previous sections, $F^-$ ions play a critical role in zeolite synthesis by stabilising small cavities and balancing the positive charge of OSDA without the need of forming defects. For this reason, the fluoride route was extensively studied by many researchers. However, in most of the studies the usual concentration of fluoride in the synthesis gel was equal to the concentration of OSDA molecules to ensure charge balance. Recently, Jo *et al.*[75] proposed the so-called 'excess fluoride' approach, which involved increasing the fluoride concentration in the synthesis gel and was shown to promote the formation of novel zeolite structures. Based on the excess fluoride approach, the group of Hong synthesised different

 

aluminosilicate zeolites, *i.e.*, ERS-7 (ESV), EMM-10P, EU-1 (EUO), MCM-22P (MWW), ZSM-12 (MTW), and ZSM-58 (DDR), that did not crystallise under normal $F^-$ concentration conditions ($F/OSDA^{q+} = q$).[76]

Similarly to the case above, decreasing zeolite stability can be deemed as a synonym of decreasing phase density, a topic of specific interest that we approach in the next section. Recently, a new rule has been established by Hong and coworkers when the F/OSDA ratio is increased from its typical value of $F/OSDA^{q+} = q$, where fluoride and OSDA are electrostatically compensated. For larger than '$q$' values, typically $2q$ or $3q$, different zeolite phases may appear, with apparently decreasing energetic stability according to computational results.[74a] Hong and co-workers synthesised several novel zeolites such as PST-21 (PWO), PST-22 (PWW), PST-24, and PST-30 (PTY) using various mono- and diquaternary imidazolium-based cations as OSDAs under excess fluoride conditions ($HF/OSDA^{q+} \geq 2q$, where $q$ is 1 or 2),[75,77] achieving new framework types with intersecting 9- and 10-ring channels that exhibit high shape-selectivity in catalytic applications, particularly in reactions like 1-butene isomerization.

In the original fluoride route to high-silica zeolites, equimolar concentrations of OSDA and $F^-$ were applied. Jo *et al.*[75] carried out a study on the concentration effect of $F^-$ in the presence of a series of well-studied imidazolium OSDAs. By using an $F^-$/OSDA ratio of 2, two new zeolites, PST-21 and PST-22, with novel topologies, PWO and PWW, were discovered. These were found to consist of non-jointly connected modified double 4-ring (*d4r*) or *bre* units, previously unseen as secondary building units. This led the authors to propose a number of new hypothetical structures containing this same secondary building unit. Using the excess fluoride strategy in combination with a computationally designed OSDA they were able to synthesise a zeolite with one of these predicted frameworks, PTY,[77] thus illustrating the targeted synthesis of a hypothetical structure by combining previous experimental insights with computer-aided OSDA design. In subsequent work, the Hong group applied the excess-fluoride strategy to synthesise a high-silica version of ERS-7 (ESV),[76a] and a zeolite intergrowth with unique structural features, PST-24.[78] A detailed study of the effects of $F^-$ concentration and Si/Al ratio in combination with a series of *n*-alkyl *n*-methyl piperidines as OSDAs illustrated how fluoride concentration is an important factor affecting phase selectivity, crystal size and Al distribution.[76b] The interplay of Al and fluoride concentrations and OSDA structure in the outcome of zeolite synthesis under excess fluoride conditions of PST-21 (PWO), PST-22 (PWW), and ERS-7 (ESV) was studied by force field calculations.[74a] While the synthesis outcomes at normal HF/OSDA = 1 were correctly predicted by the lowest synthesis energies (*e.g.*, RTH was accurately predicted as the product in aluminosilicate gels using 1,2,3-trimethylimidazolium as the OSDA, with a synthesis energy of −1.406 eV per $TO_2$), the zeolite phases formed at higher fluoride concentrations could not be explained in this line. Experimental results at higher HF/OSDA ratios were rationalised by the hypothesis that increasing $F^-$ concentration stabilises zeolite phases with increasing synthesis energies, likely due to the higher degree of mineralization provided by $F^-$ ions.[76b] For instance, when the HF/OSDA ratio was raised to 2.0, the aluminosilicate synthesis product using 1,2,3-trimethylimidazolium as OSDA changed from RTH to PWO, which had the second lowest synthesis energy (−1.137 eV per $TO_2$).

In summary, excess fluoride conditions can lead to new zeolite phases that were not previously feasible under lower fluoride concentrations, and computational methods can be used to support further studies along this route.

## 7. Density of zeolites *versus* stability

As seen above, discovery of new zeolite phases seems to have historically followed a path from higher to lower densities. For clarity, all FD discussed herein are reported consistently in units of T-atoms per 1000 Å$^3$ (T/1000 Å$^3$). Quartz and high density silica polymorphs (tridymite, cristobalite, coesite, with densities in the range 21.8–29.6 T atoms per 1000 Å$^3$)[79] were widely known and characterised in past centuries. For instance, aluminosilicate zeolites reported before 1950 are: SOD, ANA, CAN, NAT, EDI, and THO, whose densities are in the range 15.7–19.2, according to the IZA Atlas. Nowadays there are 62 structural types with density lower than 15.7 and 187 structural types in the specified range of 15.7 to 19.2 according to IZA database plus one new additional zeolite (ZMQ-1).[70] The relation between density and stability was investigated with computer simulations, first by Akporiaye and Price[24] and later by Henson, Cheetham and Gale,[80] showing a good inverse linear correlation for structures calculated as pure silica. In the meantime, the first experimental determination was made by Navrotsky and coworkers using high-temperature solution calorimetry to measure heats of formation.[81] Two force fields have been compared and found to show good accuracy with the experimental results of formation heats in pure silica zeolites.[82]

There is not a strict correlation between density and largest ring size, as can be seen from Fig. 2, since the size of all rings, not only the largest, contribute to the density. In other words, small pore zeolites (with 8-rings as largest) can have densities as low as 14.2 (LTA), 14.5 (RHO) and 15.1 (CHA), among others, whilst large pore zeolites (with 12-rings as largest) can have densities as large as 17.2 (IFR), 17.5 (OKO) and 18.2 (MTW).

A seminal study by Brunner and Meier in 1989[83] shows the counterintuitive result that low density zeolites require a large number of small rings, although – importantly – the contrary is not true, and a large number of small rings does not necessarily mean a low density. Their study demonstrates that the lowest possible framework density should decrease with the average (including multiplicities) size of the smallest ring (ASR) associated with each T site. At the time, 4-rings were the smallest known rings, leading to the conclusion that the lowest densities were found in structures where all T sites contained 4-rings. Examples include LTL (16.7), ERI (16.1), LEV (15.9), CHA (15.1), LTA (14.2), and FAU (13.3), among others. The study also successfully predicted that zeolites with FD lower than 12 could

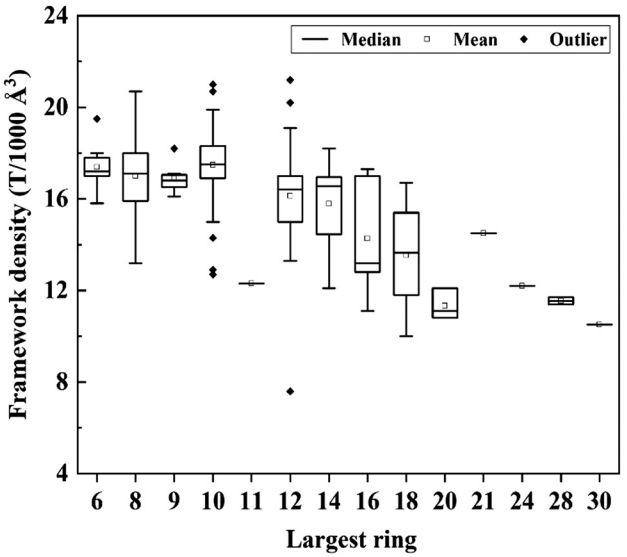


Fig. 2 Relation between zeolite framework density and largest ring, using data from IZA database with one new additional zeolite (ZMQ-1[86]) and including 260 structures.

only be achieved in structures containing 3-rings, such as, for instance, very recently, ITQ-70 (–IVY),[84] implicitly assuming synthesis *via* the hydrothermal route. However, recent advances have demonstrated that alternative synthesis methods, such as ADOR (assembly, disassembly, organisation, reassembly) and topotactic condensation, can yield unconventional zeolite phases that deviate from criteria derived from hydrothermal experiments. For instance, ZEO-5 (HZF),[85] with FD 10.8, and ZMQ-1,[86] with FD 11.4, have been obtained through synthesis routes that critically involve non-hydrothermal steps while both contain FDs lower than 12 without having 3-rings. At the time of the original study, 3-ring-containing zeolites were unknown, but this prediction was first realised just one year later with the synthesis of MEI zeolite,[87] which, despite incorporating 3-rings, still exhibited a relatively high FD (14.7), well above 12. Only two fully connected zeolites, RWY (gallium–germanium chalcogenide) and IRR (silico–germanate), as well as one interrupted framework –IRY, fulfil this criteria, with respective densities 7.6, 11.8 and 11.1. The remaining 19 zeolites with 3-rings (from a total of 23) as their smallest structural feature exhibit densities larger than 12 due to the presence of a considerably large number of T sites with smallest rings larger than 3, contributing to values of ASR between 3.5 and 3.9. Although, as said above repeatedly, there is no correlation between large pore and low density, low densities can be more probably obtained by the simultaneous presence of interrupted structures and extra-large pores.

Interrupted structures are characterised by the absence of Si atoms, leading to terminal SiOH, such as, with 4-rings as smallest: –CLO (11.1), –IRT (11.7), –ITV (10.5), –IVY (10.0), and with 3-rings as smallest –IRY (11.1). All the above structures, with densities lower than 12, are extra-large pore zeolites, with the following largest rings: 16-rings (–IRY), 18-rings (–IVY), 20-rings (–CLO and HZF), 28-rings (–IRT and ZMQ-1) and 30-rings (–ITV). Although the list of interrupted structures is rapidly growing, their number is still small (18) so as to extract general rules, but Table 1 indicates 11 of them are extra-large

Table 1 Selected properties of the 27 extra-large pore zeolites. The data source is the same with Fig. 2

| No. | IZA code | Year of discovery | Largest ring | Smallest ring | Density (T/1000 Å$^3$) | T-atom chemical composition |
|---|---|---|---|---|---|---|
| 1 | AET | 1990 | 14 | 4 | 18.2 | Al–P, Al–Si–P |
| 2 | CFI | 1997 | 14 | 4 | 16.8 | Si |
| 3 | DON | 1997 | 14 | 4 | 17.1 | Si |
| 4 | –IFT | 2015 | 14 | 3 | 12.1 | Ge–Si |
| 5 | OSO | 2001 | 14 | 3 | 13.3 | Be–Si |
| 6 | SFH | 2003 | 14 | 4 | 16.5 | B–Si |
| 7 | SFN | 2003 | 14 | 4 | 16.6 | B–Si |
| 8 | UTL | 2004 | 14 | 4 | 15.6 | Ge–Si |
| 9 | IFO | 2013 | 16 | 4 | 17.3 | Al–Si–P |
| 10 | –ION | 2020 | 16 | 4 | 17.0 | Si |
| 11 | –IRY | 2010 | 16 | 3 | 11.1 | Ge–Si |
| 12 | JZO | 2021 | 16 | 4 | 13.2 | Si–Al |
| 13 | JZT | 2023 | 16 | 4 | 12.8 | Si |
| 14 | ETR | 2003 | 18 | 4 | 15.4 | Ga–Al–Si |
| 15 | IRR | 2010 | 18 | 3 | 11.8 | Ge–Si |
| 16 | ITT | 2006 | 18 | 3 | 12.8 | Ge–Si |
| 17 | –SSO | 2014 | 18 | 4 | 16.7 | Si |
| 18 | VFI | 1988 | 18 | 4 | 14.5 | Al–P, Al–Si–P, (Fe, Co, Ti)–Al–P |
| 19 | –IVY | 2025 | 18 | 4 | 10.0 | Si |
| 20 | –CLO | 1991 | 20 | 4 | 11.1 | Ga–P, Al–P, Mn–Ga–P, Zn–Ga–P |
| 21 | HZF | 2024 | 20 | 4 | 10.8 | Si |
| 22 | –IFU | 2015 | 20 | 4 | 12.1 | Ge–Si |
| 23 | –EWT | 2014 | 21 | 4 | 14.5 | Si, Si–Al |
| 24 | –SYT | 2018 | 24 | 4 | 12.2 | Ge–Si |
| 25 | –IRT | 2011 | 28 | 4 | 11.7 | Ge–Si |
| 26 | ZMQ-1[a] | 2024 | 28 | 4 | 11.4 | Si–Al |
| 27 | –ITV | 2009 | 30 | 4 | 10.5 | Ge–Si |

[a] IZA code yet not assigned.

 

Table 2 Selected properties of the 19 lowest density zeolites. The data source is the same with Fig. 2

| No. | IZA code | Year of discovery | Largest ring | Smallest ring | Density (T/1000 Å$^3$) | T-atoms |
|---|---|---|---|---|---|---|
| 1 | RWY[a] | 2002 | 12 | 3 | 7.6 | Ga–Ge |
| 2 | –IVY | 2025 | 18 | 4 | 10.0 | Si |
| 3 | –ITV | 2009 | 30 | 4 | 10.5 | Ge–Si |
| 4 | HZF | 2024 | 20 | 4 | 10.8 | Si |
| 5 | –CLO | 1991 | 20 | 4 | 11.1 | Ga–P, Mn–Ga–P, Al–P, Zn–Ga–P |
| 6 | –IRY | 2010 | 16 | 3 | 11.1 | Ge–Si |
| 7 | ZMQ-1[b] | 2024 | 28 | 4 | 11.4 | Si–Al |
| 8 | –IRT | 2011 | 28 | 4 | 11.7 | Ge–Si |
| 9 | IRR | 2010 | 18 | 3 | 11.8 | Ge–Si |
| 10 | –IFT | 2015 | 14 | 3 | 12.1 | Ge–Si |
| 11 | –IFU | 2015 | 20 | 4 | 12.1 | Ge–Si |
| 12 | –SYT | 2018 | 24 | 4 | 12.2 | Ge–Si |
| 13 | JSR | 2013 | 11 | 3 | 12.3 | Ga–Ge |
| 14 | OBW | 2001 | 10 | 3 | 12.7 | Be–Si |
| 15 | ITT | 2006 | 18 | 3 | 12.8 | Ge–Si |
| 16 | JZT | 2023 | 16 | 4 | 12.8 | Si |
| 17 | BOZ | 2012 | 10 | 3 | 12.9 | Be–As |
| 18 | JZO | 2021 | 16 | 4 | 13.2 | Si–Al |
| 19 | TSC | 1998 | 8 | 4 | 13.2 | Si–Al |

[a] RWY is only in the form of gallium–germanium chalcogenide, while other entries have oxygen atoms connecting the tetrahedra. [b] IZA code yet not assigned.

pore. Hence 61% (11/18) of the interrupted structures are extra-large pore, and 41% (11/27) of the extra-large pore zeolites are interrupted. If synthesis methods can be driven towards new interrupted structures, it is likely that the number of extra-large pore zeolites will continue growing at an accelerated pace. Since, from Table 2, 42% (8/19) of the lowest density zeolites are interrupted, it also seems that the synthesis of new interrupted structures may lead to obtaining a large number of small density extra-large pore materials. Finally, considering that 61% (11/18) of the interrupted structures have been obtained in the last 15 years, it can be seen that there is some particular feature, that to the best of our knowledge is passing unreported, by which making new interrupted structures is becoming more frequent.

Since the nineties when extra-large pore aluminophosphate (VFI)[88] and pure silica (DON, CFI)[89] were first reported, the total number of extra-large pore zeolites (including 11 interrupted structures) is 27, of which eight are silicates (–SSO, JZT, –EWT, DON, CFI, –ION, HZF, and –IVY) and only two are aluminosilicates (JZO and ZMQ-1). Notably, there are four additional extra-large pore zeolites (ECNU-9, NUD-1, NUD-6 and ITQ-56) not included in IZA database and hence not counted. And, so far, there are no OSDA features that have been proposed for likely giving an extra-large pore zeolite as synthetic outcome, except perhaps, very recently, the introduction of large phosphonium cations, such as tricyclohexyl(methyl)phosphonium for the synthesis of JZO and bis-1,8(tricyclohexyl phosphonium) octamethylene for the synthesis of ZMQ-1. These are more thermally and chemically resistant than alkylammonium and allow to carry out the synthesis at higher temperature and longer time, without chemical degradation at high pH.

As indicated above, aluminosilicates do not seem to be an appropriate chemical composition for extra-large pore zeolites, but a reason for that has not been found in the literature. From the 27 extra-large pore zeolites, 13 have density lower than 13.0 and 10 have density larger than 15.0, which means that a large span of densities is possible. Regarding the smallest ring, only 5 zeolites have 3-ring as the smallest ring, whilst the other 22 have 4-ring as the smallest ring. As to structural units, 12 zeolites contain D4Rs whilst 15 do not contain D4Rs, meaning, overall, that conditions to have extra-large pores are not particularly stringent. Then, there is not, as far as we know at the time of writing, a structural motif or a chemical condition that is required to form an extra-large pore zeolite.

## 8. Role of Ge as structure directing agent

Introducing germanium in the synthesis of zeolites was done as early as in 1974,[90] but it took until 1998 to synthesise the first pure Ge zeolites by Li and Yaghi in 1998,[63] AST and ASV, with the latter (structurally called ASU-7) being a new topology at the time. The synthesis including Ge has allowed, so far, the synthesis of 59 zeolites (Table 3) of which 39 were new zeolites. Of these 59 Ge containing zeolites, 35 contain D4Rs, indicating a well-known preference of Ge to nucleate D4Rs.[91] Only 11 zeolites containing D4Rs (out of 45) have, so far, not been synthesised with Ge: –CLO, ACO, AFY, DFO, IFY, ITW, IWV, JZT, POR, UFI, and HZF. D4Rs can also form, among other conditions, in the presence of fluoride from silica gels (in the absence of Ge) in the following 11 cases: AST, BEC, HZF, IFY, ISV, ITH, ITW, IWR, JZT, LTA and STW. To the best of our knowledge only two structures containing D4Rs have so far been synthesised as pure silica without the presence of fluoride, JZT and HZF, through topotactic interlayer condensation and interchain-expanded synthesis strategy, respectively.[85,92]

With framework densities currently in the interval 7.6–21.2 T/1000 Å$^3$, the plot in Fig. 3a shows that Ge–zeolites are, in general,

Table 3 Selected properties of 59 Ge-containing zeolites

| No. | IZA code | Year of discovery | Largest ring | Smallest ring | Density (T/1000 Å$^3$) | T-atom chemical composition | Year of Ge–zeolite discovery | If new | If D4R |
|---|---|---|---|---|---|---|---|---|---|
| 1 | ABW | 1951 | 8 | 4 | 17.6 | Ge–Al | 2000 | No | No |
| 2 | AEL | 1986 | 10 | 4 | 19.2 | Ge–Al–P | 1997 | No | No |
| 3 | ANA | 1930 | 8 | 4 | 19.2 | Ge–Al, Ge–Ga | 1998 | No | No |
| 4 | AST | 1991 | 6 | 4 | 15.8 | Ge, Ge–Si | 1998 | No | Yes |
| 5 | ASV | 1998 | 12 | 4 | 19.1 | Ge | 1998 | Yes | Yes |
| 6 | BEC | 2000 | 12 | 4 | 15.1 | Ge, Ge–Si | 2000 | Yes | Yes |
| 7 | BOF | 1998 | 10 | 4 | 18.3 | Ge–Ga | 1998 | Yes | No |
| 8 | BOG | 1990 | 12 | 4 | 16.1 | Ge–Si–B | 2010 | No | No |
| 9 | BSV | 1998 | 12 | 4 | 18.7 | Ge–Ga | 1998 | Yes | No |
| 10 | CAN | 1930 | 12 | 4 | 16.9 | Ge–Al, Ge–Ga | 1986 | No | No |
| 11 | DFT | 1994 | 8 | 4 | 17.7 | Ge–Ga | 1998 | No | No |
| 12 | EOS | 2018 | 10 | 4 | 17.6 | Ge–Si | 2018 | Yes | Yes |
| 13 | EWO | 2017 | 10 | 5 | 19.1 | Ge–Si | 2019 | No | No |
| 14 | FAU | 1958 | 12 | 4 | 13.3 | Ge–Al, Ge–Ga | 1959 | No | No |
| 15 | GIS | 1970 | 8 | 4 | 16.4 | Ge–Al | 1999 | No | No |
| 16 | –HOS | 2021 | 12 | 4 | 14.7 | Ge–Si | 2021 | Yes | Yes |
| 17 | –IFT | 2015 | 14 | 3 | 12.1 | Ge–Si | 2015 | Yes | Yes |
| 18 | –IFU | 2015 | 20 | 4 | 12.1 | Ge–Si | 2015 | Yes | Yes |
| 19 | IRN | 2012 | 10 | 4 | 15.3 | Ge–Si | 2012 | Yes | Yes |
| 20 | IRR | 2010 | 18 | 3 | 11.8 | Ge–Si | 2010 | Yes | Yes |
| 21 | –IRT | 2011 | 28 | 4 | 11.7 | Ge–Si | 2011 | Yes | Yes |
| 22 | –IRY | 2010 | 16 | 3 | 11.1 | Ge–Si | 2010 | Yes | Yes |
| 23 | ISV | 1999 | 12 | 4 | 15.0 | Ge–Al–Si, Ge–Si | 2002 | No | Yes |
| 24 | ITG | 2012 | 12 | 4 | 16.6 | Ge–Si | 2012 | Yes | Yes |
| 25 | ITH | 2002 | 10 | 4 | 17.4 | Ge–Al–Si | 2006 | No | Yes |
| 26 | ITQ-21[98 a] | 2002 | 12 | 4 | 13.9 | Ge–Si | 2002 | Yes | Yes |
| 27 | ITR | 2008 | 10 | 4 | 17.4 | Ge–Si | 2008 | Yes | Yes |
| 28 | ITT | 2006 | 18 | 3 | 12.8 | Ge–Si | 2006 | Yes | Yes |
| 29 | –ITV | 2009 | 30 | 4 | 10.5 | Ge–Si | 2009 | Yes | Yes |
| 30 | IWR | 2003 | 12 | 4 | 15.6 | Ge–Al–Si | 2003 | Yes | Yes |
| 31 | IWS | 2008 | 12 | 4 | 14.8 | Ge–Si | 2008 | Yes | Yes |
| 32 | IWW | 2003 | 12 | 4 | 16.6 | Ge–Si | 2003 | Yes | Yes |
| 33 | JBW | 1978 | 8 | 4 | 18.8 | Ge–Al | 2000 | No | No |
| 34 | JSR | 2013 | 11 | 3 | 12.3 | Ge–Ga | 2013 | Yes | No |
| 35 | JST | 2011 | 10 | 3 | 14.3 | Ge–Ga | 2011 | Yes | No |
| 36 | LOS | 1974 | 6 | 4 | 16.9 | Ge–Al | 1978 | No | No |
| 37 | LTA | 1956 | 8 | 4 | 14.2 | Ge–Si, Ge–Al | 1959 | No | Yes |
| 38 | MON | 1990 | 8 | 4 | 17.6 | Ge–Al | 2002 | No | No |
| 39 | NAT | 1930 | 9 | 4 | 16.2 | Ge–Ga, Ge–Al | 1985 | No | No |
| 40 | POS | 2014 | 12 | 4 | 15.5 | Ge–Si | 2014 | Yes | Yes |
| 41 | PTF | 2022 | 10 | 4 | 16.0 | Ge–Si | 2022 | Yes | Yes |
| 42 | PUN | 2009 | 10 | 3 | 15.0 | Ge–Al | 2009 | Yes | No |
| 43 | RHO | 1973 | 8 | 4 | 14.5 | Ge–Al | 1999 | No | No |
| 44 | RWY | 2002 | 12 | 3 | 7.6 | Ge–Ga | 2002 | Yes | No |
| 45 | SBN | 1998 | 8 | 3 | 16.1 | Ge–Al, Ge–Ga | 1998 | Yes | No |
| 46 | SOD | 1930 | 6 | 4 | 16.7 | Ge–(Be, Al, Ga), Ge–Si–Ga–Al | 1993 | No | No |
| 47 | SOF | 2008 | 12 | 4 | 16.4 | Ge–Si | 2008 | Yes | Yes |
| 48 | SOR | 2017 | 12 | 4 | 17.1 | Ge–Si | 2017 | Yes | Yes |
| 49 | SOS | 2005 | 12 | 3 | 17.0 | Ge–B | 2005 | Yes | No |
| 50 | SOV | 2019 | 12 | 4 | 13.3 | Ge–Si | 2019 | Yes | Yes |
| 51 | STW | 2008 | 10 | 4 | 16.4 | Ge–Si | 2008 | Yes | Yes |
| 52 | SVV | 2008 | 6 | 4 | 18.0 | Ge–Si | 2008 | Yes | Yes |
| 53 | –SYT | 2018 | 24 | 4 | 12.2 | Ge–Si | 2018 | Yes | Yes |
| 54 | THO | 1933 | 8 | 4 | 15.7 | Ge–Ga | 2000 | No | No |
| 55 | UOS | 2007 | 10 | 4 | 17.6 | Ge–Si | 2007 | Yes | Yes |
| 56 | UOV | 2014 | 12 | 4 | 16.2 | Ge–Si | 2014 | Yes | Yes |
| 57 | UOZ | 2004 | 6 | 4 | 19.5 | Ge | 2004 | Yes | Yes |
| 58 | UTL | 2004 | 14 | 4 | 15.6 | Ge–Si | 2004 | Yes | Yes |
| 59 | UWY | 2010 | 12 | 4 | 16.3 | Ge–Si | 2010 | Yes | Yes |

[a] IZA code yet not assigned.

slightly more dense than Si–zeolites, with an interval (excluding outliers) of 14.2–20.2 T/1000 Å$^3$ for Si–zeolites and 15.1–19.5 T/1000 Å$^3$ for Ge–zeolites, suggesting little differences although with some higher occurrence of very low density materials among Si–zeolites.

To the question whether most of Ge- and SiGe–zeolites are large or extra-large pore zeolites, and taking into account that the largest ring goes, in general, from 6 to 30, for Ge–zeolites ($GeO_2$) the largest rings are 6 and 12; for zeolites with Ge without Si they go from 6 to 12 (6, 8, 9, 10, 11, 12), and for

 

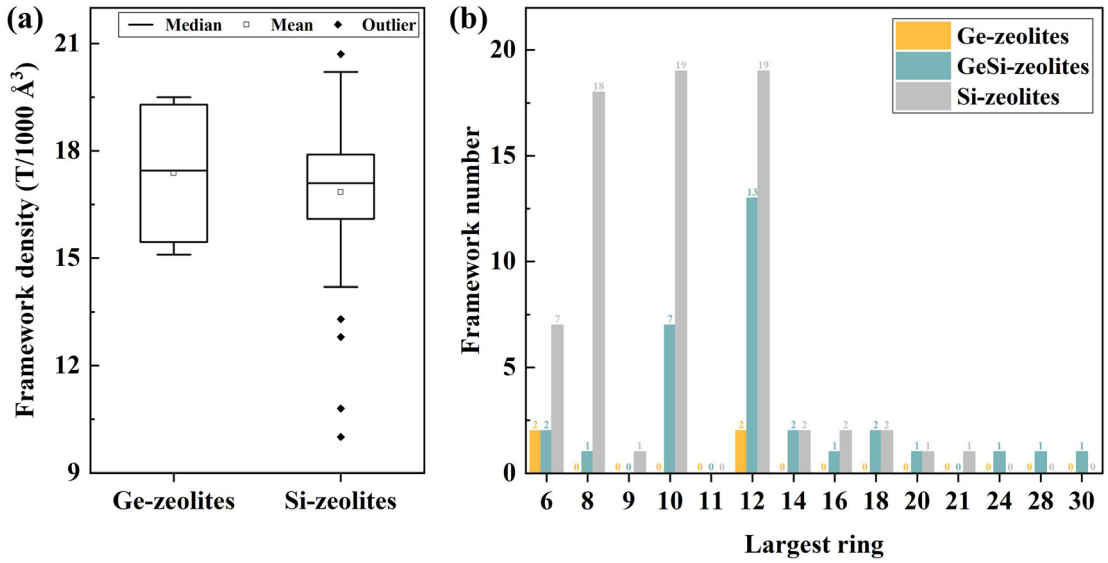


Fig. 3 (a) Framework density of $SiO_2$ and $GeO_2$ zeolites; (b) largest ring of Si-, Ge-, and SiGe–zeolites.

SiGe–zeolites they go from 6 to 30 (6, 8, 10, 12, 14, 16, 18, 20, 24, 28, 30), as can be seen from Fig. 3b. On the one hand extra-large pore zeolites can be made without Ge, but on the other hand, if we consider relative occurrence, the percentages of extra-large pore zeolites (largest ring $>12$) according to chemical composition is: 0% (Ge–zeolites, 0/4), 11.1% (Si–zeolites, 8/72), and 28.0% (SiGe–zeolites, 9/32), meaning that the participation of Si atoms is necessary and the addition of Ge atoms is beneficial to the formation of extra-large pore zeolites.

Computational studies of Ge–zeolites have nothing in particular with respect to the other chemical compositions except that there are few force fields to describe the structural and energetic features. Due to the considerably larger flexibility of Ge with respect to Si or Al, and with a much larger tendency of Ge to trigonal-bipyramid or octahedral coordination, the force constant of the O–Ge–O angle should be considerably lower than that for Si and Al. If this three-body term does not exist, the quality of the force field to reproduce structural features may suffer some inconsistency since departure from a tetrahedral network is less constrained, giving too much flexibility, and affecting structural integrity.

Efficient computational strategies such as computational chemistry-assisted design and machine learning have been carried out in the investigation of germanosilicate zeolites.[93] The computational chemistry-assisted design approach, which focuses on the interaction between OSDAs and zeolite frameworks, has proven to be effective for identifying optimal OSDAs for synthesising specific zeolites.[94] For instance, the synthesis of novel ECNU-16 and known IM-16 germanosilicates by using 1,1′-(1,4-butanediyl)-bis(3-methyl-1*H*-imidazolium) (4BI) and 1-ethyl-3-methylimidazolium (1E3MI) cations as OSDAs, respectively,[95] was theoretically verified by molecular mechanics simulations. These simulations calculated the location of OSDA molecules within zeolite channels and their interaction energies. The results revealed that 4BI exhibited a stronger interaction energy with ECNU-16, while 1E3MI showed a better interaction energy with IM-16, in excellent agreement with experiments. Using 1,3-bis(1-adamantyl)-imidazolium ($BAdaI^+$) as organic cation in fluoride media, Fu *et al.*[96] successfully synthesised high-silica IWS zeolite with Si/Ge ratios ranging from 4 to 16, marking the first time this material was obtained with Si/Ge ratios exceeding 4. To understand the reason behind this, they conducted DFT calculations to analyse the interaction energies between the OSDA and IWS framework. Their results revealed that the interaction energy between the OSDA and the zeolite framework increases with the addition of Ge atoms until a critical Si/Ge ratio is reached. For traditional OSDAs, such as 1,2-dimethyl-3-(3-methylbenzyl)-imidazolium ($DMBI^+$) and 1,3-bis-(triethylphosphoniummethyl)-benzene ($BTEP^{2+}$) the critical Si/Ge ratios were 3.5 and 4.6, respectively. In contrast, the critical Si/Ge ratio for the bulky $BAdaI^+$ was significantly higher, at 16. This explains why $BAdaI^+$ successfully directed the synthesis of high-silica IWS zeolite, as it provided stronger stabilization energy even at much lower Ge content compared to conventional OSDAs.

The machine learning strategy uses complex mathematical models to "learn" from a large set of data and has been applied to structure identification and framework classification. For example, Corma and co-workers investigated the different factors that play a role in the synthesis of ITQ-21 and ITQ-30 using principal component analysis and machine learning methods, including neural networks and decision trees.[97] Key synthesis variables, such as Al/(Si + Ge), $H_2O$/(Si + Ge), and Si/Ge ratios, were used as input parameters in the models. The models accurately predicted various outputs, including crystallinity, phase type, and structural principal components, demonstrating high predictive performance. The models also predicted the lowest Ge content of the gel (Si/Ge = 37.5) for the synthesis of ITQ-21 zeolite with high crystallinity, which was in agreement with the literature.

## 9. OSDA design and specificity

As discussed in Section 2, the interaction energy between an OSDA and a zeolite, also termed the stabilisation energy, is readily calculated by molecular simulations. It is generally observed that, when a given zeolite is formed in the presence of an OSDA, the corresponding stabilisation energy is favourable. However, a favourable stabilisation energy does not guarantee that a particular zeolite will be obtained in practice. In this section we discuss efforts to rationalise and predict why, depending on the synthesis conditions,

(a) a particular OSDA can lead to several zeolites, and

(b) a particular zeolite can be obtained with several OSDAs.

Situation (a) pertains to OSDA specificity, and situation (b) is of importance for OSDA design.

One example of OSDA specificity is the trispyrrolidinium-MEI system mentioned in Section 3, where ZSM-18 is formed almost exclusively in the presence of this OSDA under a broad range of synthesis conditions. The origin of this specificity as well as the observed Al siting could be traced back by detailed molecular modelling of the zeolite–OSDA interactions.[32] In a study directed towards the synthesis of boggsite (BOG), multiple OSDAs were considered that were known to direct the synthesis of zeolites with similar intersecting 10- and 12-ring channels.[99] While a number of OSDAs were predicted to have favourable stabilisation energies to fit into the BOG framework, it was found eventually that a phosphazene produced the target zeolite, with other OSDAs leading to different zeolites. Another example of OSDA specificity is 1-isopropyl-4,4,7-trimethyl-4-azonia-tricyclo[5.2.2.0] undecane-8-ene, in an experimentally tested computational study of OSDAs targeting two structurally related zeolites, ISV and BEC. The different energetic terms defining the zeolite–OSDA stabilisation energy were analysed to rationalise the specificity of this OSDA towards ISV. *N*,*N*,*N*′,*N*′-tetraethyl bicyclo[2.2.2]-oct-7-ene-2*R*,3*S*:5*R*,6*S*-dipyrrolidium was found to specifically direct the synthesis to MCM-68, crystallising the large-pore three-dimensional framework MSE.[100] It must be noted that, since some of these OSDAs are difficult to synthesise, the observed specificity can be in part due to the fact they have not been used frequently. On the other hand, some OSDAs have been utilised commonly in the synthesis of zeolites due to their ease of synthesis even though they show minimal specificity. For instance, hexamethonium is a widely used OSDA for the zeolite synthesis due to its availability and versatility. However, it is a very flexible compound with a long alkyl chain which allows it to adapt to different zeolite pore and channel geometries, making it less selective for a specific zeolite framework. As a result, hexamethonium is associated with the synthesis of up to 10 different zeolite phases (BEA, BEC, EUO, EZT, ITH, IWR, IWW, MFI, *STO and UOZ), as documented in the OSDB database.[27]

In computational OSDA design we can distinguish multiple objectives:

(i) For a known zeolite that has been synthesised before, alternative OSDAs can be designed that make the synthesis of the same zeolite more economically feasible, or that produce the zeolite with a different chemical composition.

(ii) The outcome of experiments where several OSDAs produce several zeolites can be rationalised by calculating thermodynamic descriptors. These typically are based upon the zeolite–OSDA van der Waals interaction energy, but other descriptors have also been investigated.

(iii) The design of OSDAs to synthesise previously unknown zeolites or known zeolites with a new chemical composition.

Case (i) in which alternative OSDAs for an existing zeolite are designed is both a simple as well as useful example in which calculations give valuable information. Casci and coworkers designed,[101] based on the original decamethonium OSDA, pentane-l,5-bis(methylpyrrolidinium) for the synthesis of NU-87 (NES), but this was only achieved when a gallium aluminosilicate gel was used. Instead, for an aluminosilicate gel, the new zeolite NU-88 was synthesised. Since its structure was never provided by the authors it is not possible to test if pentane-l,5-bis(methylpyrrolidinium) fits better in NU-88 than in NU-87. It is always the case that competition between zeolite phases can never be excluded when an OSDA for a target zeolite is designed, and hence if the calculations with all OSDAs include only the target zeolite, the agreement with experiment, if found, can be considered fortunate. Similar work along this approach was made by searching OSDAs for aluminosilicate AEI,[102] silica STW,[21,103] aluminosilicate SWY, with *d6r*, *gme* and *swy* cavities, in combination with $K^+$,[104] aluminosilicate AFX, with *d6r*, *gme* and *aft* cavities (SSZ-16, Si/Al = 13),[105] silicate and aluminosilicate ITR using $Me_4Et_2$-diquat-6, compared to $Me_6$-diquat-6 employed in the related ITH zeolite, and considerably different to propane-1,3-bis(trimethylphosphonium), the original OSDA employed in the synthesis of silicogermanate ITR.[106]

Selective OSDAs, *i.e.* those giving only one zeolite, have always attracted attention since this is one of the holy grails of zeolite synthesis. However, OSDAs are never the only synthesis variable and hence it is almost impossible that variation of other synthesis conditions (presence of inorganic cations, pH, time, stirring, synthesis gel, chemical composition) does not change the zeolite phase obtained. Rigidity of the OSDA, once suggested to be a key parameter for selectivity, is not always linked to selectivity. *N*,*N*,*N*-trimethyladamantammonium, initially giving only silica CHA (SSZ-13) and supposed to be a selective OSDA, was reported to give another four zeolite phases (STT, AFI, MWW, *STO) a few years after the first report.[4] On the other hand, some flexible OSDAs (TPA, TBA) have been found to be quite selective, hence concluding we need to be careful to link OSDA rigidity and zeolite phase selectivity. OSDA specificity can be argued to be provisional until more experiments using such OSDA are performed. Sometimes OSDA specificity is observed for commonly obtained zeolite phases such as AEI, BEA, MOR, or MFI. These frameworks can be considered as default phases that are easily formed under a given set of synthesis conditions and that do not need specific structure-direction.[15,72] The OSDAs in these cases are not actually required for their templating, and they are ineffective for the synthesis of any other zeolite. OSDA specificity does also depend on the zeolite micropore: zeolites with similar micropores (such as ITE and RTH) are unlikely to be synthesised with

 

a specific OSDA, and a number of OSDAs (such as 1-ethyl-1,2-dimethylpiperidinium or 1,1-diethyldecahydro-1*H*-1-benzazepinium) give both ITE and RTH. In fact, a large family of imidazolium OSDAs has been found to synthesise RTH in a variety of synthesis conditions.[107] This was attributed to the strong interaction energies, calculated by force field simulations, between imidazolium ions, especially 1,2-dimethylimidazolium ($-18.3$ kJ mol$^{-1}$), and 1,2,4,5-tetramethyl imidazolium ($-20.0$ kJ mol$^{-1}$), compared to the original OSDA of RTH, *N*-ethyl-*N*-methyl-5,7,7-trimethylazoniumbicyclo[4.1.1]octane ($-11.1$ kJ mol$^{-1}$), and the ability of RTH to pack 4 imidazolium ions per unit cell (32 T-atoms per u.c.), enabling the framework to incorporate a higher content of Al atoms than its competitors such as ITW (2 OSDA per u.c., 24 T-atoms), FER (4 OSDA per u.c., 36 T-atoms), and TON (2 OSDA per u.c., 24 T-atoms). When assessing the stabilities of zeolites using their novel synthesis energy approach, Altundal *et al.*[25] observed that the structure with the ability to incorporate more Al atoms has a more favourable synthesis energy, making it the synthesis product. This trend can be attributed to two reinforcing effects. First, as the Al content increases, the framework develops a greater negative charge, which enhances Coulombic interactions with the positively charged OSDAs. Second, an increase in Al content requires a higher concentration of OSDAs to maintain charge balance, leading to denser OSDA packing within the zeolite pores. This enhanced packing leads to more pronounced vdW interactions between the OSDAs and the framework, further stabilizing the structure. Together, these effects highlight the necessity of considering both electrostatic and dispersion interactions when assessing the energetic stability of zeolite synthesis.

From our extensive search we suggest 1,3,5-tris(1,2-dimethylimidazolium) benzene, that has only produced IWR, is an excellent and rare example of specific OSDA in which there is an accurate match between the branched shapes of both OSDA and micropore (Fig. 4).

The studies representing Case (ii), where several OSDAs are utilised to synthesise various zeolites, give much more valuable information and are more realistic for targeted zeolite synthesis since not only one zeolite is taken into consideration. In other words, OSDAs should not only fit well in the target zeolite but also should fit badly in all other zeolites. An outstanding study by Wagner *et al.*[109] highlights the influence of OSDA size and aluminium content on zeolite formation. Small OSDA molecules typically favour the formation of clathrate structures, such as NON. As the OSDA size exceeds the cage dimensions of clathrates, one-dimensional channel-type zeolites begin to form, particularly under low aluminium contents. At higher aluminium concentrations in the synthesis gel, the products shift toward multidimensional zeolites such as MFI, CHA, and AEI. Furthermore, mono- and bicyclic quaternised amines preferentially form SSZ-36, an intergrowth of ITE and RTH zeolites, at high lattice substitution conditions, while tri- and tetracyclic OSDAs tend to form open-framework structure STF due to its larger pore size. These findings highlight the critical role of OSDA size in directing zeolite synthesis. Importantly, vdW interactions between OSDAs and zeolite frameworks, calculated by force field simulations, were consistent with experimental results, confirming the observed trends. Also, Roslova *et al.*[19] investigated the vdW interaction energies between six known OSDAs for SSZ-43 (structure unveiled but IZA code not assigned) and six OSDAs associated with one of its competing phases, *STO, using molecular modelling. SSZ-43, a partially disordered zeolite with 1-D 12-ring channels, competes with *STO and STF during synthesis. Their results showed a good correlation between phase selectivity and zeo–OSDA vdW interactions. Based on this, they calculated the vdW interaction energies of SSZ-43, *STO, and STF with a library of long-chain diquaternary OSDAs which were hypothesised to more effectively stabilise SSZ-43 due to a better shape and size match between the OSDAs and the zeolite framework. Out of $\sim$300 molecules, two diquats were identified and successfully used

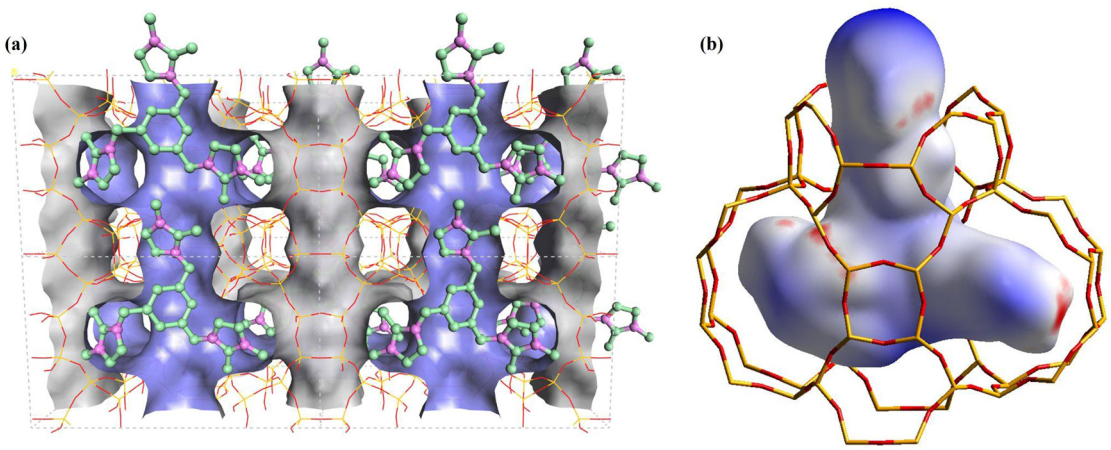


Fig. 4 (a) Configuration of 1,3,5-tris(1,2-dimethylimidazolium) benzene (hydrogen atoms omitted for clarity) occluded in the micropores (shaded) of IWR zeolite. (b) Hirshfeld surface of 1,3,5-tris(1,2-dimethylimidazolium) benzene occluded in IWR. The red and blue areas indicate intermolecular contacts shorter and longer than the sum of the van der Waals radii of the atoms, respectively, while the white area represents the intermolecular contacts around the sum of van der Waals radii. Modified from Fig. 8 in ref. 108.

for the targeted synthesis of SSZ-43. Even when there is no zeo–OSDA specificity, a detailed analysis and the adequate selection of descriptors, including the classic zeo–OSDA vdW interactions, can help to design better OSDAs for the synthesis of competing zeolites.

From the experimental viewpoint Case (iii), has been at play for the last three of four decades. However, in most studies the structure of the unknown zeolite was not known *a priori*, and its synthesis was the result of a more or less unexplored choice of both OSDAs and synthesis conditions. Many new zeolites have been synthesised using novel OSDAs and this remains an exciting challenge, as the number of new zeolites keeps growing steadily without an indication that a plateau has been reached.

Targeted design of an OSDA to synthesise an unknown zeolite with a hypothetical, *a priori* predicted structure has not yet been reached routinely by computational studies, and this remains indeed the holy grail of new and increasingly sophisticated computational studies. Efforts towards this end started in 1999[110] when the first database of hypothetical zeolites appeared. This was the result of a mathematical breakthrough which allowed to define a unique code for zeolites in an exclusive and necessary basis such that a systematic variation of codes allowed to generate the corresponding list of zeolites.[111] A number of other databases followed,[112] as well as a number of force field based computational studies that defined criteria of feasibility under pure silica and aluminosilicate composition.[82,113]

One study aimed at generating a hypothetical zeolite framework selected from the Hypothetical Zeolites Structures database[114] was reported by Boruntea *et al.*[115] The hypothetical zeolite was chosen based upon energetic and geometrical criteria, as well as on its expected performance in deNOx and MTO catalysis. OSDAs were initially selected by considering the structures of known OSDAs that synthesise cages similar in size to those present in the hypothetical zeolite. A final selection of three OSDAs was made based upon their predicted van der Waals interaction energies with the zeolite. Subsequent experiments exploring a variety of synthesis conditions did not produce the targeted zeolite, but instead generated a competing zeolite, ERI, including a previously unknown high-silica variant. This outcome could be partially rationalised by van der Waals stabilisation energy calculations, and at the same time hinted at the limitation of exclusively relying on energetic considerations for OSDA design.

A first successful attempt to synthesise a zeolite with a priorly predicted framework topology was reported by Jo and Hong.[77] The starting point of this study was the discovery of two novel zeolites using the excess fluoride approach, PST-21 and PST-22.[75] The previously unobserved building block observed in these new zeolites was used to generate 10 hypothetical zeolite frameworks. A series of diazolium di-cations were then designed with similar size and shape as the OSDAs used to synthesise PST-21 and PST-22. The van der Waals stabilisation energies of 32 designed OSDAs in the 10 hypothetical zeolites and in PST-21 and PST-22 were calculated, and 7 diazolium di-cations with the lowest stabilisation energy in at least one of the hypothetical zeolites were selected for synthesis. One of these led to the synthesis of the target zeolite, characterised as PST-30.

## 10. Self-assembling OSDAs

The first observation of self-assembling organics in zeolites was reported, as far as we know, in the group of Davis.[116] They investigated the motion and distribution of organic species (*i.e.*, hexamethylbenzene (HMB), adamantane, and naphthalene) adsorbed within the cavities of Na–Y, and found HMB to self assembly in pairs inside the supercages. To the best of our knowledge it is not until 2004 that, without explicit mention, self-assembly was described in detail by Gómez-Hortigüela *et al.* for the synthesis of AlPO-5 (AFI) using benzylpyrrolidinium as OSDA.[117] This study investigated the structure-directing role of five OSDAs containing benzyl rings in the synthesis of AFI zeotypes with AlPO (AlPO-5) and SAPO (SAPO-5) compositions. While all the OSDAs successfully directed the synthesis of AlPO-5, only benzylpyrrolidine and dibenzyldimethylammonium predominantly facilitated the formation of SAPO-5. Computational results revealed that the most stable arrangement of the monobenzyl OSDAs (benzylpyrrolidine, benzylpiperidine, and benzylhexamethylenimine) involved dimerization, which maximised packing efficiency and was crucial for forming the large 12-ring channels of the AFI structure. Furthermore, the calculated interaction energies of the monobenzyl OSDAs with the AFI framework followed the order: benzylpyrrolidine > benzylpiperidine > benzylhexamethylenimine explaining why benzylpyrrolidine was most effective in directing SAPO-5 synthesis.

Self-assembly was also applied for the elusive synthesis of pure silica LTA (called ITQ-29) using julolidine as OSDA in 2004,[118] and in 2015 using a novel imidazolium based OSDA,[119] with the latter including a computational study. The stabilisation energies, calculated using force field simulations, showed that the interaction between the novel imidazolium-based cation and the LTA framework, incorporating two molecules per cavity (16.9 kJ $mol^{-1}$ per Si), was stronger than that of julolidine (14.3 kJ $mol^{-1}$ per Si). Furthermore, the results highlighted that dimerization of julolidine is crucial for the successful formation of the LTA framework. Without proper dimerization, the stabilisation energy of julolidine was significantly lower (−7.4 kJ $mol^{-1}$ per Si), which favoured the competing formation of other phases, such as AST.

An excellent study has unveiled that OSDA–OSDA interactions are crucial in the directing effect of the well-known case of TEA in the synthesis of beta zeolite.[120] An aggregate of six TEA cations has been proposed to be responsible to nucleate an ordered silica–alumina arrangement resembling a fragment of the final material corresponding to the channel intersection of zeolite beta.

Self-assembly constitutes a considerable challenge for *a priori* computational studies aimed to guess OSDA loading in zeolite micropores, since this leads to a rather large OSDA packing of molecules in a situation in which OSDA–OSDA interactions become attractive in spite of the electrostatic cation–cation

 

repulsion. For instance, OSDB failed to report the correct loading of benzylpyrrolidinium in AFI[121] and julolidine in LTA,[122] both resulting in the wrong prediction of absent self-assembly.

## 11. Role of defects as structure directing agent

Simply speaking the role of Al and defects are closely related since both of them compensate for the positive charge of OSDAs, and hence both of them are expected to be in close proximity to such positive charge. But, whilst much attention has been dedicated in literature to study Al location, defects have been so far largely unexplored, and it is only recently that a growing interest is shown. The presence of zeolite internal defects can be better understood in pure silica zeolites which, by not having trivalent atoms, can only compensate the positive charge of the organic or inorganic SDAs (ISDAs) by forming siloxy and silanol groups, $\equiv SiO^- \cdots HOSi \equiv$, also called a 1 : 1 connectivity defect, always vicinal since they are formed by breaking a SiOSi bond in the presence of hydroxide or water:

$$\equiv SiOSi \equiv + OH^- \rightarrow \equiv SiO^- + HOSi \equiv$$

$$\equiv SiOSi \equiv + H_2O \rightarrow 2 \equiv SiOH$$

If the two reactions above break two neighbour SiOSi bonds, a 'connectivity defect' containing three silanols and one siloxy, also called a 3 : 1 defect, is formed. Alternatively, a 3 : 1 defect can also be formed around a vacant Si in the framework ('vacancy defect'), as indicated in Scheme 1 of ref. 28. Hence two types, connectivity defects and vacancy defects, have so far been proposed.

Defects do not only form to compensate for the positive charge of the OSDA but also as a consequence of intrinsic strain of the zeolite framework in specific crystallographic positions and can also be neutral if two silanols are formed instead of siloxy + silanol. In the above two cases defects do not lead to a tetrahedral vacancy, but defects can also be formed with a tetrahedral vacancy according to the following reactions:

$$Si(OSi \equiv)_4 + 2H_2O \rightarrow 4 \equiv SiOH + SiO_2$$

$$Si(OSi \equiv)_4 + OH^- + H_2O \rightarrow 3 \equiv SiOH + \equiv SiO^- + SiO_2$$

The connectivity defect made by three silanols and one siloxy (3 : 1 defect) has been characterised in as-made silica ZSM-5 using tetrapropylammonium in the work by Koller *et al.*,[123] as well as Brunklaus *et al.*[124] using $^{29}Si$ and $^{1}H$ double and triple quantum (DQ, TQ) NMR. Both studies were able to find the precise location of the defect and indicate the presence of four fused 6-rings as a favourable condition for the stabilisation of this type of defect. Using this defect location, protruding slightly outside of the micropore channel, a recent computational study suggests that the self-diffusivity of benzene is slightly faster compared to that of the defectless silicalite,[125] due to a slightly larger pore volume and partial access to micropore corrugations in the former. Previous experimental results agree with such interpretation,[126] perhaps counterintuitive since the expected behaviour is that defects may hinder diffusivity. More recent studies also point to the importance of defects, differently affecting the diffusivities of adsorbates in a separation process.[127] Far from claiming that this is a general trend, it becomes clear that defects may not only affect the catalytic properties but also the properties related to separation and diffusion.

Another important point to consider is the difference between the number of defects before and after zeolite calcination. Calcination not only removes the OSDA, at temperatures typically between 500 and 800 °C, but also transfers the positive charge from the OSDA to the zeolite framework by either generating a Brønsted acid site, SiO(H)Al, if a trivalent atom is present, or else protonating a siloxy that becomes a silanol group. In the latter case, during calcination, an undetermined number of connectivity defects can be healed according to the following reaction:

$$2 \equiv SiOH \rightarrow \equiv SiOSi \equiv + H_2O$$

And indeed it is not unusual that the number of defects of the calcined sample is lower than that of the as-synthesised.[128]

The synthesis of SSZ-74 (–SVR)[129] was a considerable achievement since it is, so far, the only one in which the defects are localised in a well determined crystallographic position with 100% occupancy. Hence, unlike other interrupted structures in which $Q^3$ sites are terminating groups without any possible framework continuation, in SSZ-74 $Q^3$ sites are generated by a Si vacancy in a fully coordinated zeolite. This unique structural property of SSZ-74 also allows testing the hypothesis of proximity between the siloxy defects and the positive charge of the OSDAs. If the position of OSDAs is ordered and found by XRD, its proximity to these defects can be examined. Isaac *et al.*[130] used Rietveld refinement techniques, revealing that the OSDAs (*i.e.*, 1,6-bis(*N*-methylpyrrolidinium)hexane and 1-methyl-1-[6-(trimethylazaniumyl)hexyl]pyrrolidinium) in SSZ-74 are located within the undulated 10-ring channels along the [110] direction adopting an energetically favourable linear conformation, with their hydrogen atoms interacting with both silanol groups and framework oxygen atoms (Fig. 5).

## 12. Inorganic plus organic SDAs

Ever since the first synthetic zeolite, structure-directing properties of inorganic cations have been utilised in zeolite synthesis. However, after the introduction of methylammonium cations to the synthetic route by Barrer and Denny in early 1960s,[1] scientists started focusing more on the OSDAs which allow controlling the zeolite pore size and shape. In addition, using OSDAs, it was possible to synthesise zeolite phases that were never obtained before. However, this was not exclusive to OSDAs, as ISDAs have also contributed to the discovery of new zeolite structures. A typical example is LTA, which does

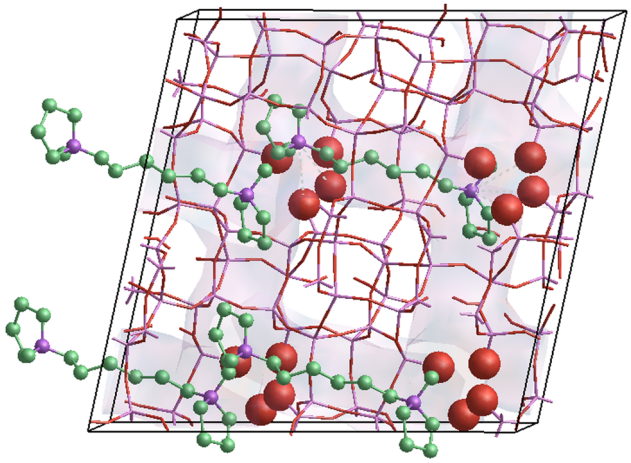

Fig. 5 Location of 1,6-bis(*N*-methylpyrrolidinium)hexane (H atoms omitted for clarity) in the micropore (shaded) of siliceous SSZ-74, with the short distance between siloxy or silanol oxygens (large red balls) and quaternary nitrogens (purple balls) of the OSDA highlighted (dotted lines) for the central molecule. Geometry taken from ref. 130.

not occur naturally and was first synthesised using inorganic cations.[131] Nevertheless, the importance of ISDAs has been rediscovered and is now a growing focus of research, especially for their role in working together with OSDAs to synthesise new zeolites with better stabilities.[132] Guo *et al.*[133] investigated the structural similarities of PAU, MWF and RHO structures which were revealed to be an expanded or modified version of the others, sharing common building units. They identified a hierarchical expansion mechanism where the frameworks grow through the addition of specific cage units, such as *pau* and *d8r* cages, along unit-cell edges. Based on this, they predicted the structures of PST-20 and PST-25 which were even more expanded and complex versions of the RHO family. Since PAU and MWF structures were synthesised using TEA combined with $Na^+$ cations they anticipated the novel zeolites PST-20 and PST-25 could also be synthesised with the same OSDAs. Moreover, they included $Ca^{2+}$ and/or $Sr^{2+}$ cations in the synthesis, since these cations were known to favour the formation of *t-gsm*, *t-oto* and *t-phi* cages which were abundant in the targeted zeolites. Using this approach, it was possible to obtain pure PST-20 zeolite using TEA as OSDA and a combination of $Na^+$ and $Sr^{2+}$ cations as ISDA, whereas PST-25 crystallised with the addition of $Ca^{2+}$ to the synthesis gel. Building on this work, Shin *et al.*[134] predicted and synthesised even more complex RHO family zeolites, PST-26 and PST-28. These novel structures were synthesised using TEA as OSDA and $Na^+$ and $Ca^{2+}$ cations as ISDAs, similar to the methodology used for PST-20 and PST-25. Notably, the synthesis was only successful when the $H_2O/SiO_2$ ratio was below 34.7, aligning with the Villaescusa rule, which states that lower water concentrations favour the formation of lower-density zeolites. These studies highlighted the effectiveness of employing multiple inorganic cations in zeolite synthesis.

In 2004, Lewis *et al.*[135] introduced the charge density mismatch (CDM) approach, which facilitated co-templating with multiple SDAs, both organic and inorganic, in zeolite synthesis. This method involves using a CDM OSDA, an OSDA with low charge density (such as TEA), in a synthesis gel with a low Si/Al ratio. On its own, the charge mismatch prevents TEA from crystallizing any zeolite. However, by introducing crystallizing SDAs with higher charge densities, such as TMA or $Na^+$ cations, they successfully synthesised zeolites UZM-5 and UZM-9. Notably, the synthesis of UZM-4 required $Li^+$ cations instead of $Na^+$, highlighting the critical role of specific charge-density interactions in directing zeolite formation. Chawla *et al.*[136] investigated the cooperative effects of two OSDAs, TPA and cetyltrimethylammonium (CTA), in combination with two ISDAs, $Na^+$ and $K^+$, on ZSM-5 crystallization using experimental and computational methods. Results showed that TPA, the most commonly used OSDA for ZSM-5 synthesis, facilitates relatively fast ZSM-5 crystallization in the presence of $Na^+$, while $K^+$ cations hinder the formation of ZSM-5 (MFI) zeolite when paired with TPA. In contrast, CTA, a less conventional OSDA, when combined with $K^+$, resulted in faster crystallization of ZSM-5. Molecular dynamics simulations revealed that TPA preferentially occupies the intersections of straight and sinusoidal channels, directing aluminium to these specific sites and causing zoned aluminium distributions. On the other hand, CTA, due to its flexible chain structure, can occupy either straight or sinusoidal channels, allowing a more uniform aluminium incorporation throughout the ZSM-5 framework. These results suggest that CTA offers a cost-effective and efficient alternative to TPA as OSDA in the synthesis of ZSM-5, especially in combination with $K^+$, making it a valuable option for tailoring zeolite properties in industrial applications.

## 13. Big data and artificial intelligence for better OSDA design and specificity

Artificial intelligence (AI) algorithms like natural language processing allow to exploit and organise the massive amount of experimental data on zeolite synthesis that are available. This has enabled the construction of databases of curated zeolite synthesis and property data in machine readable formats, which in turn has led to the development of workflows exploiting these data for OSDA design.[137] While force field and *ab initio* techniques like molecular dynamics and DFT have proven their value in the design of OSDA candidates for templating zeolites, these methods are computationally intensive and focus on a single zeolite target. Machine–learning algorithms and methods allow the development of more efficient modelling approaches to the computational design of OSDAs. *De novo* design algorithms, originally developed for drug design, have been applied to automatised computational OSDA design. Lately, generative neural networks to generate and optimise molecules have been making their way into OSDA design.[138] At the time of submission of this tutorial, a review covering the state-of-the-art of AI methods in predicting zeolite properties, development and use of machine–learning (ML) potentials for zeolite simulations, generative modelling, and

 

aiding experimental synthesis, has appeared.[139] Limitations and the strategies to overcome them are discussed. The main challenges identified are data quality and availability, the shortcomings of currently used descriptors, the applicability across different structures, the interpretability of the ML models, and the synthesizability of structures obtained from generative modelling. An interesting view is given on how LLMs (large language models) and metaverse technology could be deployed in a future platform for the digital design of zeolites.

An in-depth treatment of the subjects treated in this paragraph can be found in ref. 140.

### 13.1 Databases and artificial intelligence

In ref. 141, a workflow is presented that uses natural language processing (NLP) and text parsing tools to extract synthesis data from a collection of 70 000 zeolite papers and organise these into a format suitable for automated data analysis and machine learning. The extracted data included gel compositions, crystallization conditions, OSDAs used and the resulting zeolite or amorphous phases. Pairwise relationships between the raw data reflected known trends in zeolite synthesis, indicating the reliability of the extraction pipeline. The potential use of the database for studying more complex relationships between synthesis conditions and resulting zeolite topologies was illustrated by predicting the framework density of Ge containing zeolites.

Muraoka *et al.*[142] compiled a dataset of 22 crystalline zeolite phases and 626 OSDA-free synthesis conditions and explored several machine learning algorithms and synthesis parameters to predict synthesis outcome. The synthesis parameters included synthesis temperature, heating time and chemical composition. Analysis of the machine learning models allowed to rationalise physicochemical structural and empirical insights such as solubility, Ostwald's step rule, Löwenstein's rule and structural similarity between zeolite frameworks. The weights of the synthesis parameters in the machine–learning models were used to derive a structural similarity measure between the zeolites, allowing to construct a similarity network of zeolites that was extended to include frameworks not in the original data set and that showed the formation of communities of both structurally and synthetically similar materials. Peng *et al.*[143] report machine–learning prediction of pore-size and framework densities of germanosilicate zeolites on experimental data on 876 synthetic routes. As input features, both gel composition and OSDA descriptors were used, and several machine–learning methods were explored. It was found that the use of WHIM (Weighted Holistic Invariant Molecular)[144] descriptors for the OSDAs in combination with tree-based regression models were most successful in predicting both pore-sizes and framework densities, and these models were verified using a set of 66 new experiments which were not present in the original data set. A method was introduced to visualise and analyse the contribution of the WHIM descriptors through an extension of SHAP (SHapley Additive exPlanations). The interpretability of the models allowed to identify key synthesis descriptors that influence synthesis outcome.

An overview of how machine–learning integrates into high-throughput discovery of zeolites is presented by Moliner *et al.*[145] High-throughput synthesis and characterization platforms are described, and data-mining techniques applied to analyse the results are illustrated by means of several published studies. An overview is given of computational methods that implement machine–learning for hypothetical structure generation and phase characterization, for characterizing zeolite–OSDA interaction and designing OSDAs, and for automated literature data extraction.

In the work of Jensen *et al.*,[146] the NLP and text mining tools developed in ref. 141 were used to compile a comprehensive database of 5665 synthesis routes comprising OSDAs, zeolite phases and gel chemistry. The OSDAs were encoded with WHIM descriptors and relationships between the OSDAs and their target zeolite phases were visualised by dimension reduction. In addition, a generative neural network was built to generate novel OSDAs for given targets. The input of the network consisted of structural data of the zeolites in the data set, and the corresponding one-hot coded synthesis parameters. The network was trained using the SMILES (Simplified Molecular Input Line Entry System) encoded OSDAs. The trained network was then applied for structure generation to generate OSDAs directed towards CHA and SFW frameworks.[147] For CHA, molecules were generated with very similar structural features to known OSDAs. For SFW, generated structures were evaluated with molecular mechanics simulations and shown to have more favourable binding energies than the known OSDAs for this framework.

To investigate which strategy for high-throughput calculation of OSDA–zeolite stabilization energies is most adept in a high-throughput setting, Schwalbe-Koda *et al.*[148] performed a benchmark of 272 zeolite–OSDA pairs. The methods tested included both static and dynamic and DFT and DREIDING force field calculations in combination with various relaxation schemes to extract a value for the stabilization energies. It was found that the stabilization energies obtained with the force field frozen pose method correlate best with the values obtained with DFT. In this method, a local molecular mechanics minimization of a OSDA–zeolite pose is carried out at constant unit cell volume. The stabilization energy is then obtained by taking the difference between the energy of the minimised OSDA–zeolite complex and the energies of the individual zeolite and OSDA components. Hereby the structures of the zeolite and OSDA are not individually relaxed. This scheme is computationally less costly than molecular dynamics or DFT calculations and can be applied to high-throughput computational screening of OSDAs. It was subsequently applied in ref. 27, where a computational pipeline was set up to calculate stabilization energies of a set of 549 OSDAs extracted from literature toward 209 zeolite frameworks with the aim to predict phase competition in OSDA directed zeolite synthesis, that is, why a given OSDA directs the synthesis to a particular zeolite framework in favour of a competing one. Starting from the premise that selective OSDAs bind strongly to one zeolite framework and bind weakly to competing frameworks, directivity, competitivity and

templating energy metrics obtained from the binding energy matrix were defined. In addition, OSDA volume and shape descriptors, defined by the largest distances along the principal axes in a 2D projection of the OSDA structure, were calculated. These data, together with literature references were collected in a navigable database, the OSDB[149] to enable interactive computer-augmented design of OSDAs. The use of the database was illustrated by several examples. These included synthesis of zeolites SSZ-39 (AEI) and SSZ-13 (CHA), fine tuning the charge distribution of an OSDA to modify the Al distribution in aluminosilicate CHA zeolite, and synthesis of a CHA/AEI intergrowth, with newly designed OSDAs. For the design of OSDAs for intergrowths, the OSDB and the shape matching procedures were used to search for OSDAs that have a dual specificity towards the intergrowth target, as detailed by Bombarelli and coworkers.[150] The possible application of the binding energy data in the OSDB in combination with OSDA volume and shape analysis to the repurposing of OSDAs, and their selection for dual-OSDA syntheses, is examined in ref. 151.

In the ZeoSyn database[152] parameters of 23 961 zeolites synthesis data have been extracted from the zeolite literature published over a time span of 50 years. The synthesis parameters include gel composition in terms of molar ratios of heteroatoms, mineralizing agents, metal cations and OSDAs, reaction temperature and time, and descriptors of OSDAs used in the syntheses. The data set consisted of 23 961 synthesis routes encompassing 233 zeolite topologies and 921 OSDAs. A random forest model was trained with the set of 43 parameters to predict the resulting zeolite framework for each data point. The data set included failed syntheses, and the model was tested using a random split with a 80/20 train/test ratio. For 73% of the synthesis routes in the test set the experimentally observed framework was correctly predicted. In addition to providing a tool to predict synthesis outcomes, the classification model was analysed to give deeper insights into the impact of the synthesis parameters on the zeolite products formed.

### 13.2 ML prediction of binding energies

As discussed in Section 2 of this tutorial, the interaction energy between an OSDA and its target zeolite, also termed the stabilization energy, to a large extent predicts the ability of the OSDA to synthesise a zeolite. An example of a software suite to calculate this stabilization energy, zeoTsda, is described in ref. 153. The method starts with a Monte Carlo calculation to fit a single, rigid copy of an OSDA into the unit cell of a rigid target zeolite framework by evaluating the van der Waals energy between the OSDA and the zeolite. The best scoring configuration is relaxed using a full molecular mechanics lattice energy minimization and the resulting OSDA–zeolite van der Waals interaction is used to assess the templating ability of the OSDA towards the target zeolite. In order to speed up the calculation to allow high-throughput evaluation of OSDAs a single OSDA copy per unit cell was used. It was benchmarked on experiments involving the synthesis of the competing zeolites BOG and ITQ-45, and further tested on a set of OSDAs and 221 zeolites. In spite of the approximations used, the methodology allows to identify suitable OSDAs for a given target zeolite and to predict what competing frameworks may be involved. As the calculation of zeolite–OSDA stabilization energies is very computationally intensive, replacement of atomistic calculations by machine–learning algorithms has been undertaken to enable the screening of large numbers of molecules as putative OSDAs.

In the work of Daeyaert *et al.*,[154] a set of 4781 OSDA-BEA stabilization energies obtained by molecular dynamics simulations in previous design studies were used to train and validate a neural network to predict the stabilization energies using a linear encoding of the 3D OSDA structures as diffraction patterns.[155] The machine–learning algorithm sped up the calculation of stabilization energies by two orders of magnitude and was used in the *de novo* design of novel OSDAs targeting BEA. Similarly, Galvez-Llompart and Sastre used a neural network with 2D and 3D molecular topology descriptors to predict stabilization energies in BEA, which was then used to screen a large number of available compounds as OSDA towards this target.[156] The massive screening of the chemical space formed by quaternary ammonium compounds against all known zeolite frameworks using an artificial neural network to predict stabilization energies will be described in the next section.[157]

### 13.3 *De novo* design and generative modelling

In a *de novo* design algorithm, molecules with desirable properties are automatically generated.[158] *De novo* design originated in computational drug design to generate molecules that bind to a biological target. *De novo* design was first applied to the design of OSDAs for zeolites with the ZEBEDDE program.[159] In this program, putative OSDAs are computationally grown by joining chemical fragments and positioning these in a target zeolite. An evolutionary algorithm drives the formation of molecules that optimally fill the cavities in the target zeolite while avoiding overlap between the van der Waals spheres of the OSDA and the zeolite. The ZEBEDDE program was successfully applied to design novel OSDAs to synthesise known zeolite frameworks.[160] A *de novo* design program that addresses the synthetic accessibility of the designed compounds and that allows the use of external, independent software to evaluate the resulting molecules was adapted for OSDA design in Michael Deem's laboratory.[161] The program was used to design experimentally confirmed novel OSDAs templating STW,[103] AEI[102] and CHA[20] zeolites. The algorithm is based upon a multifunctional optimization algorithm, allowing the design of OSDAs that selectively synthesise one zeolite framework and not a competing one,[162] or that selectively synthesise one enantiomer of a chiral zeolite.[163] It was also illustrated how *de novo* design can be used to design OSDAs for selected zeolite frameworks, including hypothetical ones, predicted to be interesting materials in specific adsorption and separation applications.[164] A related design method is virtual combinatorial chemistry, where novel molecules are generated by combining a set of available reagents into a given reaction scheme. An example of a reaction scheme leading to quaternary ammonium OSDAs is given in Scheme 1.

 

$$R_1NH_2 + R_2X \rightarrow R_1R_2NH \rightarrow R_1R_2N^+Me_2$$

Scheme 1 Synthesis of quaternary ammonium OSDAs by alkylation of a primary amine with a halide, yielding a secondary amine, followed by successive methylation steps to form the quaternary ammonium cation. (X = halogen, Me = $CH_3$).

When the number of available reagents becomes large, and the reaction scheme contains multiple steps, the total number of possible reaction products gets too large to evaluate computationally or even to enumerate, and stochastic search algorithms need to be applied to search this huge chemical space. One such approach is ant colony optimization (ACO), a nature-inspired stochastic optimization algorithm based on the behaviour of ant colonies searching for food.[165] In ACO, artificial 'ants' explore a search space and through communication by 'pheromones' discover paths that lead to highly promising areas in this search space. This method is particularly effective for solving complex combinatorial problems, such as molecular design, where exhaustive enumeration is impractical. Muraoka *et al.*[166] cast the virtual combinatorial chemistry problem into a network-based problem for which the ant algorithm has been shown to be very efficient. They applied a similar virtual reaction scheme, with multiple alkylation steps to react with all free N orbitals on the amine, to computationally design OSDAs directed to the synthesis of CHA, AEI and CON zeolites. The number of reaction products that can be obtained with this reaction scheme using commercially available amine and alkyl halides is too large for an exhaustive exploration with molecular dynamics simulations to calculate the zeolite–OSDA stabilisation energies. Therefore, an ant colony optimization algorithm was devised to efficiently search this vast chemical space. In addition to the zeolite–OSDA stabilisation energies and simple chemical heuristics, a cost efficiency parameter was introduced to search for OSDAs that are both effective and economically feasible. Application of this multi-objective design algorithm to the three target zeolites generated known, experimentally proven OSDAs, as well as structural analogues of known molecules and completely novel structures.

A massive exhaustive combinatorial chemistry study of OSDAs towards known zeolites was recently carried out by Xie *et al.*[157] Putative OSDAs were generated by an exhaustive enumeration of quaternary ammonium compounds that can be generated by the nucleophilic aliphatic substitution reaction between commercially available amines and halides. The resulting chemical space contained 543 174 mono quaternary and 1 793 915 diquaternary ammonium compounds, and was characterised in terms of synthesizability, cost and diversity. To predict the binding affinity to all known zeolites of this huge amount of OSDAs, a total of nearly 500 million zeolite–molecule pairs had to be screened. To make this computationally feasible, the force field energy calculation was replaced by machine–learning (ML). ML learning models were trained, validated and tested using a large body of binding energy calculations obtained in previous work.[27,146] Input to the ML models were physical descriptors of both OSDAs and zeolite frameworks. It was found that an ensemble of multiple multilayer perceptron (MLP) models showed the best performance in correctly predicting the binding energies of OSDAs in known zeolites. The ensemble MLP model was then used to exhaustively screen the library of hypothetical quaternary ammonium compounds to obtain the predicted binding energies of all ~500 million compounds towards 216 known zeolites. The results were applied to identify OSDAs for two known frameworks, ERI and CHA, that were experimentally shown to synthesise their target zeolites in novel chemical compositions. While developing the ML models, it was observed that they were unable to predict binding energies of OSDAs to zeolites left out of the training and test sets, indicating that further research is needed on the representation of zeolite descriptors for identifying new OSDAs for hypothetical zeolites.

About one and a half decade ago, new developments in deep neural networks caused a revolution in the analysis of image, text and audio data, and soon found their way to applications in molecular and material science.[167] In addition to their use for classification and regression, deep neural networks have been developed for generative modelling, that is, the generation of novel, unseen data after first training a neural network. Deep generative modelling of molecules was first described by Bombarelli *et al.*,[168] and a review of this emerging field can be found in ref. 138. The application of a generative neural network for OSDA design in ref. 146 was discussed above. An alternative model, using the same data set but with fewer parameters and higher computational efficiency is described by Zhong and coworkers.[169] The model architecture is evaluated on CHA and AEI subsets of the database and is shown to generate novel molecules that exhibit similar and lower stabilization energies than OSDAs in the training set. Challenges in generative modelling of molecules include addressing synthesizability of the generated molecules and interfacing molecule generation with property prediction and are the subject of current research.[170]

## 14. Conclusions

In this review, we summarised the impact of structure directing agents, including the organic and inorganic SDA, Al atoms, Ge atoms, defects, fluoride and other factors affecting the zeolite stability. Computational simulations have been employed to clarify the relation between SDA and zeolite and demonstrate the crucial role of SDA in the process of synthesising zeolites.

Recent advances in the application of big data and computational methods have significantly improved our understanding of how OSDAs influence zeolite synthesis and phase selectivity. Starting from the widely employed and simplistic van der Waals zeo–OSDA intermolecular energy, the implementation of increasingly accurate and comprehensive descriptors such as 'total energy' and 'synthesis energy' is helping to provide a wider view of the synthesis process. Among other descriptors, 'total energy' allows to bring the role of zeolite stability into the factors determining the phase selectivity so that it is no longer a matter of the OSDA only. The more recently introduced concept of, 'synthesis energy' contains the 'total energy' and adds the role of

the enthalpy of reaction throughout the contributions of the energetics of reactants. This allows to compare across different chemical compositions of the starting gel, and also allows to incorporate silica and aluminosilicate compositions in the presence of fluoride and/or siloxy/silanol defects that compensate for the positive charge of the OSDA.

Looking ahead, future research should aim to address the limitations in current models, such as the impact of water/silica ratio, kinetic factors, and long-range structural effects in the synthesis process. Greater attention should also be paid to defect characterization and the role of entropy in framework formation, as these factors play a critical role in the phase selectivity of zeolites. The use of robust computational models that are validated by experiments will be crucial in guiding the synthesis of zeolites with tailored properties for catalysis and separation applications.

The integration of machine learning and artificial intelligence has accelerated progress in OSDA design and zeolite discovery. Generative modelling and database-driven approaches have rationalised the identification of new OSDAs and hypothetical zeolite frameworks. These computational tools have successfully predicted novel combinations of zeolites and OSDAs, validated experimentally, thereby reducing the reliance on trial-error methods. However, challenges remain, including ensuring the synthesizability of computationally proposed OSDAs and aligning predictive models with real-world synthesis outcomes. Recent attempts with state of the art machine–learning tools to predict stabilization energies or other templating descriptors of OSDAs across frameworks have not been successful yet. A breakthrough here could help to reach the long outstanding goal of designing OSDAs to produce new hypothetical zeolites that are waiting to be discovered.

In conclusion, the synergy between experimental and computational methods, coupled with advances in AI and big data, is changing zeolite science. These developments not only deepen our understanding of synthesis mechanisms but also pave the way for the targeted design of next-generation materials with exceptional precision and efficiency.

## Author contributions

All authors have contributed to the whole manuscript and have given approval to the final version of the manuscript.

## Data availability

No primary research results, software or code have been included and no new data were generated or analysed as part of this review.

## Conflicts of interest

There are no conflicts to declare.

## Acknowledgements

Financial support by the Spanish Ministry of Science and Innovation (Severo Ochoa) is greatly acknowledged. G. S. thanks GVA for PROMETEO/2021/077 project as well as ASIC-UPV and SGAI-CSIC for the use of computational facilities. X. T. thanks the support by National Natural Science Foundation of China (no. 22202215). We thank an anonymous reviewer for very insightful comments on how to improve this review.

## Notes and references

1 R. M. Barrer and P. J. Denny, *J. Chem. Soc.*, 1961, 971–982.
2 R. Aiello and R. Barrer, *J. Chem. Soc.*, 1970, 1470–1475.
3 G. Kokotailo, P. Chu, S. Lawton and W. Meier, *Nature*, 1978, **275**, 119–120.
4 A. W. Burton and S. I. Zones, *Stud. Surf. Sci. Catal.*, 2007, **168**, 137–179.
5 R. Boyett, A. Stevens, M. Ford and P. Cox, *Zeolites*, 1996, **17**, 508–512.
6 V. Shen and A. T. Bell, *Microporous Mater.*, 1996, **7**, 187–199.
7 M. E. Davis and R. F. Lobo, *Chem. Mater.*, 1992, **4**, 756–768.
8 Y. Kubota, M. M. Helmkamp, S. I. Zones and M. E. Davis, *Microporous Mater.*, 1996, **6**, 213–229.
9 A. V. Goretsky, L. W. Beck, S. I. Zones and M. E. Davis, *Microporous Mesoporous Mater.*, 1999, **28**, 387–393.
10 (*a*) A. Rojas, E. Martínez-Morales, C. M. Zicovich-Wilson and M. A. Camblor, *J. Am. Chem. Soc.*, 2012, **134**, 2255–2263; (*b*) A. Rojas, M. L. San-Roman, C. M. Zicovich-Wilson and M. A. Camblor, *Chem. Mater.*, 2013, **25**, 729–738.
11 A. P. Stevens, A. M. Gorman, C. M. Freeman and P. A. Cox, *J. Chem. Soc., Faraday Trans.*, 1996, **92**, 2065–2073.
12 M. Jorge, S. M. Auerbach and P. A. Monson, *J. Am. Chem. Soc.*, 2005, **127**, 14388–14400.
13 A. A. Bertolazzo, D. Dhabal and V. Molinero, *J. Phys. Chem. Lett.*, 2022, **13**, 977–981.
14 K. Ata, T. Mineva and B. Alonso, *Molecules*, 2024, **29**, 4489.
15 A. Moini, K. Schmitt, E. Valyocsik and R. Polomski, *Zeolites*, 1994, **14**, 504–511.
16 C. M. Zicovich-Wilson, F. Gándara, A. Monge and M. A. Camblor, *J. Am. Chem. Soc.*, 2010, **132**, 3461–3471.
17 S. L. Njo, J. H. Koegler, H. van Koningsveld and B. van de Graaf, *Microporous Mater.*, 1997, **8**, 223–229.
18 Y. Ma, X. Tang, J. Hu, Y. Ma, W. Chen, Z. Liu, S. Han, C. Xu, Q. Wu, A. Zheng, L. Zhu, X. Meng and F. S. Xiao, *J. Am. Chem. Soc.*, 2022, **144**, 6270–6277.
19 M. Roslova, V. J. Cybulskis, M. E. Davis, S. I. Zones, X. Zou and D. Xie, *Angew. Chem., Int. Ed.*, 2022, **61**, e202115087.
20 T. M. Davis, A. T. Liu, C. M. Lew, D. Xie, A. I. Benin, S. Elomari, S. I. Zones and M. W. Deem, *Chem. Mater.*, 2016, **28**, 708–711.
21 C. Shi, L. Li, L. Yang and Y. Li, *Chin. Chem. Lett.*, 2020, **31**, 1951–1955.
22 Z. Shi, L. Wang, Q. Deng, L. Han, C. Liu, T. Liu, C. Gong, W. Deng, J. Liu and Y.-A. Zhu, *Fuel*, 2025, **381**, 133274.

 

23 C. X. Gong, K. K. Zhu, M. Lei, X. G. Zhou, D. Chen and Y. A. Zhu, *Ind. Eng. Chem. Res.*, 2024, **63**, 16770–16778.
24 D. Akporiaye and G. Price, *Zeolites*, 1989, **9**, 321–328.
25 O. F. Altundal, S. Leon and G. Sastre, *J. Phys. Chem. C*, 2023, **127**, 10797–10805.
26 G. Sastre, S. Leiva, M. J. Sabater, I. Gimenez, F. Rey, S. Valencia and A. Corma, *J. Phys. Chem. B*, 2003, **107**, 5432–5440.
27 D. Schwalbe-Koda, S. Kwon, C. Paris, E. Bello-Jurado, Z. Jensen, E. Olivetti, T. Willhammar, A. Corma, Y. Roman-Leshkov, M. Moliner and R. Gomez-Bombarelli, *Science*, 2021, **374**, 308–315.
28 S. Leon and G. Sastre, *J. Phys. Chem. C*, 2022, **126**, 2078–2087.
29 T. T. Le, A. Chawla and J. D. Rimer, *J. Catal.*, 2020, **391**, 56–68.
30 K. Mlekodaj, J. Dedecek, V. Pashkova, E. Tabor, P. Klein, M. Urbanova, R. Karcz, P. Sazama, S. R. Whittleton, H. M. Thomas, A. V. Fishchuk and S. Sklenak, *J. Phys. Chem. C*, 2019, **123**, 7968–7987.
31 D. F. Shantz, C. Fild, H. Koller and R. F. Lobo, *J. Phys. Chem. B*, 1999, **103**, 10858–10865.
32 M. J. Sabater and G. Sastre, *Chem. Mater.*, 2001, **13**, 4520–4526.
33 G. Sastre, V. Fornes and A. Corma, *J. Phys. Chem. B*, 2002, **106**, 701–708.
34 Q. Wu, H. Luan and F. S. Xiao, *Natl. Sci. Rev.*, 2022, **9**, nwac023.
35 B. Lu, T. Kanai, Y. Oumi and T. Sano, *J. Porous Mater.*, 2007, **14**, 89–96.
36 S. Sklenak, J. Dědeček, C. Li, B. Wichterlová, V. Gábová, M. Sierka and J. Sauer, *Angew. Chem., Int. Ed.*, 2007, **46**, 7286–7289.
37 J. Dědeček, D. Kaucky and B. Wichterlova, *Microporous Mesoporous Mater.*, 2000, **35**, 483–494.
38 P. Sazama, J. Dědeček, V. Gabova, B. Wichterlova, G. Spoto and S. Bordiga, *J. Catal.*, 2008, **254**, 180–189.
39 K. Muraoka, W. Chaikittisilp and T. Okubo, *J. Am. Chem. Soc.*, 2016, **138**, 6184–6193.
40 T. Matsuoka, L. Baumes, N. Katada, A. Chatterjee and G. Sastre, *Phys. Chem. Chem. Phys.*, 2017, **19**, 14702–14707.
41 J. R. Di Iorio and R. Gounder, *Chem. Mater.*, 2016, **28**, 2236–2247.
42 C. T. Nimlos, A. J. Hoffman, Y. G. Hur, B. J. Lee, J. R. Di Iorio, D. D. Hibbitts and R. Gounder, *Chem. Mater.*, 2020, **32**, 9277–9298.
43 X. Gao, S. Yeo, R. Gounder, A. Moini and W. F. Schneider, *Chem. Mater.*, 2024, **36**, 11558–11569.
44 Y. Román-Leshkov, M. Moliner and M. E. Davis, *J. Phys. Chem. C*, 2011, **115**, 1096–1102.
45 K. Muraoka, W. Chaikittisilp, Y. Yanaba, T. Yoshikawa and T. Okubo, *Angew. Chem., Int. Ed.*, 2018, **57**, 3742–3746.
46 T. Biligetu, Y. Wang, T. Nishitoba, R. Otomo, S. Park, H. Mochizuki, J. N. Kondo, T. Tatsumi and T. Yokoi, *J. Catal.*, 2017, **353**, 1–10.
47 T. Liang, J. Chen, Z. Qin, J. Li, P. Wang, S. Wang, G. Wang, M. Dong, W. Fan and J. Wang, *ACS Catal.*, 2016, **6**, 7311–7325.
48 E. M. Flanigen and R. L. Patton, *US Pat.*, US4073865A, 1978.
49 J. Guth, H. Kessler, J. Higel, J. Lamblin, J. Patarin, A. Seive, J. Chezeau and R. Wey, *Zeolite Synthesis*, ACS Symposium Series, ACS Publications, 1989, vol. 398, ch. 13, pp. 176–195, DOI: **10.1021/bk-1989-0398.ch013**.
50 L. A. Villaescusa and M. A. Camblor, *Recent Res. Dev. Chem.*, 2003, **1**, 93–141.
51 A. Corma, M. Puche, F. Rey, G. Sankar and S. J. Teat, *Angew. Chem.*, 2003, **115**, 1188–1191.
52 P. A. Barrett, T. Boix, M. Puche, D. H. Olson, E. Jordan, H. Koller and M. A. Camblor, *Chem. Commun.*, 2003, 2114–2115.
53 L. A. Villaescusa, P. A. Barrett and M. A. Camblor, *Angew. Chem., Int. Ed.*, 1999, **38**, 1997–2000.
54 L. A. Villaescusa, P. A. Barrett and M. A. Camblor, *Chem. Commun.*, 1998, 2329–2330.
55 A. Cantín, A. Corma, S. Leiva, F. Rey, J. Rius and S. Valencia, *J. Am. Chem. Soc.*, 2005, **127**, 11560–11561.
56 M. Moliner, J. Gonzalez, M. T. Portilla, T. Willhammar, F. Rey, F. J. Llopis, X. Zou and A. Corma, *J. Am. Chem. Soc.*, 2011, **133**, 9497–9505.
57 D. L. Dorset, G. J. Kennedy, K. G. Strohmaier, M. J. Diaz-Cabañas, F. Rey and A. Corma, *J. Am. Chem. Soc.*, 2006, **128**, 8862–8867.
58 Z. R. Gao, S. R. Balestra, J. Li and M. A. Camblor, *Angew. Chem.*, 2021, **133**, 20411–20414.
59 Y. Yun, M. Hernández, W. Wan, X. Zou, J. L. Jordá, A. Cantín, F. Rey and A. Corma, *Chem. Commun.*, 2015, **51**, 7602–7605.
60 L. Tang, L. Shi, C. Bonneau, J. Sun, H. Yue, A. Ojuva, B. L. Lee, M. Kritikos, R. G. Bell, Z. Bacsik, J. Mink and X. Zou, *Nat. Mater.*, 2008, **7**, 381–385.
61 Y. Mathieu, J. L. Paillaud, P. Caullet and N. Bats, *Microporous Mesoporous Mater.*, 2004, **75**, 13–22.
62 T. Conradsson, M. Dadachov and X. Zou, *Microporous Mesoporous Mater.*, 2000, **41**, 183–191.
63 H. Li and O. Yaghi, *J. Am. Chem. Soc.*, 1998, **120**, 10569–10570.
64 M. J. Diaz-Cabañas, M. A. Camblor, Z. Liu, T. Ohsuna and O. Terasaki, *Mater. Chem.*, 2002, **12**, 249–257.
65 P. Caullet, J. L. Paillaud, A. Simon-Masseron, M. Soulard and J. Patarin, *C. R. Chim*, 2005, **8**, 245–266.
66 H. Koller, A. Wölker, L. Villaescusa, M. J. Díaz-Cabañas, S. Valencia and M. A. Camblor, *J. Am. Chem. Soc.*, 1999, **121**, 3368–3376.
67 C. M. Zicovich-Wilson, M. L. San-Román, M. A. Camblor, F. Pascale and J. S. Durand-Niconoff, *J. Am. Chem. Soc.*, 2007, **129**, 11512–11523.
68 A. Pulido, A. Corma and G. Sastre, *J. Phys. Chem. B*, 2006, **110**, 23951–23961.
69 M. A. Camblor, L. A. Villaescusa and M. J. Díaz-Cabañas, *Top. Catal.*, 1999, **9**, 59–76.
70 C. Baerlocher and L. B. McCusker, Database of Zeolite Structures, **https://www.iza-structure.org/databases/**, (accessed 10/05/2025).
71 Some useful crystallographic software, **https://www.iza-structure.org/IZA-SC_Software.php**, (accessed 10/05/2025).

72 P. Lu, L. A. Villaescusa and M. A. Camblor, *Chem. Rec.*, 2018, **18**, 713–723.
73 L. Villaescusa, P. Barrett, M. Kalwei, H. Koller and M. A. Camblor, *Chem. Mater.*, 2001, **13**, 2332–2341.
74 (*a*) O. F. Altundal and G. Sastre, *J. Phys. Chem. C*, 2023, **127**, 15648–15656; (*b*) K. C. Kemp, O. F. Altundal, D. Jo, W. Huang, Q. Wang, F. Deng, G. Sastre and S. B. Hong, *Chem. Sci.*, 2025, **16**, 7579–7589.
75 D. Jo, G. T. Park, J. Shin and S. B. Hong, *Angew. Chem.*, 2018, **130**, 2221–2225.
76 (*a*) J. Bae and S. B. Hong, *Chem. Commun.*, 2018, **54**, 10997–11000; (*b*) J. Bae and S. B. Hong, *Microporous Mesoporous Mater.*, 2021, **327**, 111422.
77 D. Jo and S. B. Hong, *Angew. Chem.*, 2019, **131**, 13983–13986.
78 D. Jo, J. Zhao, J. Cho, J. H. Lee, Y. Liu, C. J. Liu, X. Zou and S. B. Hong, *Angew. Chem., Int. Ed.*, 2020, **59**, 17691–17696.
79 T. Demuth, Y. Jeanvoine, J. Hafner and J. Angyan, *J. Phys.: Condens. Matter*, 1999, **11**, 3833.
80 N. J. Henson, A. K. Cheetham and J. D. Gale, *Chem. Mater.*, 1994, **6**, 1647–1650.
81 I. Petrovic, A. Navrotsky, M. E. Davis and S. I. Zones, *Chem. Mater.*, 1993, **5**, 1805–1813.
82 Y. G. Bushuev and G. Sastre, *J. Phys. Chem. C*, 2010, **114**, 19157–19168.
83 G. O. Brunner and W. M. Meier, *Nature*, 1989, **337**, 146–147.
84 J. I. Tirado, A. Sala, A. Bordes, P. P. Das, L. Palatinus, S. Nicolopoulos, J. L. Jordá Moret, A. Vidal-Moya, T. Blasco, G. Sastre, S. Valencia and F. Rey, *Angew. Chem.*, 2024, e202416515.
85 Z. R. Gao, H. Yu, F. J. Chen, A. Mayoral, Z. Niu, Z. Niu, X. Li, H. Deng, C. Marquez-Alvarez, H. He, S. Xu, Y. Zhou, J. Xu, H. Xu, W. Fan, S. R. G. Balestra, C. Ma, J. Hao, J. Li, P. Wu, J. Yu and M. A. Camblor, *Nature*, 2024, **628**, 99–103.
86 P. Lu, J. Xu, Y. Sun, R. Guillet-Nicolas, T. Willhammar, M. Fahda, E. Dib, B. Wang, Z. Qin and H. Xu, *Nature*, 2024, **636**, 368–373.
87 K. D. Schmitt and G. J. Kennedy, *Zeolites*, 1994, **14**, 635–642.
88 M. E. Davis, C. Saldarriaga, C. Montes, J. Garces and C. Crowdert, *Nature*, 1988, **331**, 698–699.
89 (*a*) C. Freyhardt, M. Tsapatsis, R. Lobo, K. Balkus Jr and M. Davis, *Nature*, 1996, **381**, 295–298; (*b*) M. Yoshikawa, P. Wagner, M. Lovallo, K. Tsuji, T. Takewaki, C. Y. Chen, L. W. Beck, C. Jones, M. Tsapatsis, S. I. Zones and M. E. Davis, *J. Phys. Chem. B*, 1998, **102**, 7139–7147.
90 L. Lerot, G. Poncelet and J. Fripiat, *Mater. Res. Bull.*, 1974, **9**, 979–987.
91 (*a*) M. O'keeffe and O. Yaghi, *Chem. – Eur. J.*, 1999, **5**, 2796–2801; (*b*) T. Blasco, A. Corma, M. J. Díaz-Cabañas, F. Rey, J. A. Vidal-Moya and C. M. Zicovich-Wilson, *J. Phys. Chem. B*, 2002, **106**, 2634–2642.
92 J. Li, Z. R. Gao, Q. F. Lin, C. Liu, F. Gao, C. Lin, S. Zhang, H. Deng, A. Mayoral, W. Fan, S. Luo, X. Chen, H. He, M. A. Camblor, F. J. Chen and J. Yu, *Science*, 2023, **379**, 283–287.
93 M. Opanasenko, M. Shamzhy, Y. Wang, W. Yan, P. Nachtigall and J. Čejka, *Angew. Chem., Int. Ed.*, 2020, **59**, 19380–19389.
94 Y. Li, H. Cao and J. Yu, *ACS Nano*, 2018, **12**, 4096–4104.
95 L. Xu, L. Zhang, J. Li, K. Muraoka, F. Peng, H. Xu, C. Lin, Z. Gao, J. G. Jiang and W. Chaikittisilp, *Chem. – Eur. J.*, 2018, **24**, 9247–9253.
96 W. Fu, W. Hu, C. Hu, Y. Wang, J. Ai, Z. Wang, C. Wang and W. Yang, *Inorg. Chem.*, 2024, **63**, 16908–16917.
97 A. Corma, M. Moliner, J. M. Serra, P. Serna, M. J. Díaz-Cabañas and L. A. Baumes, *Chem. Mater.*, 2006, **18**, 3287–3296.
98 A. Corma, M. J. Díaz-Cabañas, J. Martínez-Triguero, F. Rey and J. Rius, *Nature*, 2002, **418**, 514–517.
99 R. Simancas, D. Dari, N. Velamazan, M. T. Navarro, A. Cantin, J. L. Jorda, G. Sastre, A. Corma and F. Rey, *Science*, 2010, **330**, 1219–1222.
100 D. L. Dorset, S. C. Weston and S. S. Dhingra, *J. Phys. Chem. B*, 2006, **110**, 2045–2050.
101 J. Casci, P. Cox, R. Henney, S. Maberly and M. Shannon, *Studies in Surface Science and Catalysis*, Elsevier, 2004, vol. 154, pp. 110–117.
102 J. E. Schmidt, M. W. Deem, C. Lew and T. M. Davis, *Top. Catal.*, 2015, **58**, 410–415.
103 J. E. Schmidt, M. W. Deem and M. E. Davis, *Angew. Chem.*, 2014, **126**, 8512–8514.
104 R. G. Chitac, J. Bradley, N. D. McNamara, A. Mayoral, A. Turrina and P. A. Wright, *Chem. Mater.*, 2021, **33**, 5242–5256.
105 S. Han, W. Rao, J. Hu, X. Tang, Y. Ma, J. Du, Z. Liu, Q. Wu, Y. Ma and X. Meng, *Appl. Catal., B*, 2023, **332**, 122746.
106 Y. Ma, J. Hu, K. Fan, W. Chen, S. Han, Q. Wu, Y. Ma, A. Zheng, E. Kunkes, T. De Baerdemaeker, A. N. Parvulescu, N. Bottke, T. Yokoi, D. E. De Vos, X. Meng and F. S. Xiao, *J. Am. Chem. Soc.*, 2023, **145**, 17284–17291.
107 J. E. Schmidt, M. A. Deimund, D. Xie and M. E. Davis, *Chem. Mater.*, 2015, **27**, 3756–3762.
108 A. Pinar, L. McCusker, C. Baerlocher, J. Schmidt, S. J. Hwang, M. Davis and S. Zones, *Dalton Trans.*, 2015, **44**, 6288–6295.
109 P. Wagner, Y. Nakagawa, G. S. Lee, M. E. Davis, S. Elomari, R. C. Medrud and S. Zones, *J. Am. Chem. Soc.*, 2000, **122**, 263–273.
110 O. D. Friedrichs, A. W. Dress, D. H. Huson, J. Klinowski and A. L. Mackay, *Nature*, 1999, **400**, 644–647.
111 A. W. Dress, D. H. Huson and E. Molnár, *Acta Crystallogr., Sect. A: Found. Crystallogr.*, 1993, **49**, 806–817.
112 (*a*) Y. Li, J. Yu and R. Xu, *J. Appl. Crystallogr.*, 2012, **45**, 855–861; (*b*) M. D. Foster, A. Simperler, R. G. Bell, O. D. Friedrichs, F. A. A. Paz and J. Klinowski, *Nat. Mater.*, 2004, **3**, 234–238; (*c*) D. J. Earl and M. W. Deem, *Ind. Eng. Chem. Res.*, 2006, **45**, 5449–5454.
113 (*a*) Y. Li, J. Yu and R. Xu, *Angew. Chem., Int. Ed.*, 2013, **52**, 1673–1677; (*b*) M. W. Deem, R. Pophale, P. A. Cheeseman and D. J. Earl, *J. Phys. Chem. C*, 2009, **113**, 21353–21360; (*c*) R. Pophale, P. A. Cheeseman and M. W. Deem, *Phys. Chem. Chem. Phys.*, 2011, **13**, 12407–12412.
114 Atlas of Prospective Zeolite Structures, **https://www.hypotheticalzeolites.net/**, (accessed 18/12/2024).

 

115 C.-R. Boruntea, G. Sastre, L. F. Lundegaard, A. Corma and P. N. Vennestrøm, *Chem. Mater.*, 2019, **31**, 9268–9276.
116 S. B. Hong, H. M. Cho and M. E. Davis, *J. Phys. Chem.*, 1993, **97**, 1622–1628.
117 (*a*) L. Gómez-Hortigüela, F. Corà, C. R. A. Catlow and J. Pérez-Pariente, *J. Am. Chem. Soc.*, 2004, **126**, 12097–12102; (*b*) L. Gómez-Hortigüela, J. Pérez-Pariente, F. Corà, C. R. A. Catlow and T. Blasco, *J. Phys. Chem. B*, 2005, **109**, 21539–21548.
118 A. Corma, F. Rey, J. Rius, M. J. Sabater and S. Valencia, *Nature*, 2004, **431**, 287–290.
119 B. W. Boal, J. E. Schmidt, M. A. Deimund, M. W. Deem, L. M. Henling, S. K. Brand, S. I. Zones and M. E. Davis, *Chem. Mater.*, 2015, **27**, 7774–7779.
120 T. Ikuno, W. Chaikittisilp, Z. Liu, T. Iida, Y. Yanaba, T. Yoshikawa, S. Kohara, T. Wakihara and T. Okubo, *J. Am. Chem. Soc.*, 2015, **137**, 14533–14544.
121 Benzylpyrrolidinium in AFI, **https://zeodb.mit.edu/affinity/AFI/CWEGCQIIDCZZED-UHFFFAOYNA-N**, (accessed 18/12/2024).
122 Julolidine in LTA, **https://zeodb.mit.edu/affinity/LTA/MDWZIHPBIGDFDH-UHFFFAOYNA-N**, (accessed 18/12/2024).
123 H. Koller, R. F. Lobo, S. L. Burkett and M. E. Davis, *J. Phys. Chem.*, 1995, **99**, 12588–12596.
124 G. Brunklaus, H. Koller and S. I. Zones, *Angew. Chem., Int. Ed.*, 2016, **55**, 14459–14463.
125 A. Misturini, O. F. Altundal, P. García-Aznar, S. Kariminasab and G. Sastre, *Chem. Ing. Tech.*, 2023, **95**, 1768–1776.
126 A. Vidoni, P. I. Ravikovitch, M. Afeworki, D. Calabro, H. Deckman and D. Ruthven, *Microporous Mesoporous Mater.*, 2020, **294**, 109818.
127 Y. Fan, X. Tang, J. Hu, Y. Ma, J. Yang, F. Liu, X. Yi, Z. Liu, L. Song, A. Zheng and Y. Ma, *Nat. Commun.*, 2024, **15**, 7961.
128 J. Chezeau, L. Delmotte, J. Guth and Z. Gabelica, *Zeolites*, 1991, **11**, 598–606.
129 C. Baerlocher, D. Xie, L. B. McCusker, S. J. Hwang, I. Y. Chan, K. Ong, A. W. Burton and S. I. Zones, *Nat. Mater.*, 2008, **7**, 631–635.
130 C. Isaac, I. Deroche, J. L. Paillaud, T. J. Daou, A. Ryzhikov, L. Michelin, S. Rigolet, L. Josien and H. Nouali, *Cryst. Growth Des.*, 2021, **21**, 4013–4022.
131 T. B. Reed and D. Breck, *J. Am. Chem. Soc.*, 1956, **78**, 5972–5977.
132 (*a*) J. Shin, D. Jo and S. B. Hong, *Acc. Chem. Res.*, 2019, **52**, 1419–1427; (*b*) H. Luan, Q. Wu, J. Wu, X. Meng and F. S. Xiao, *Chin. J. Struct. Chem.*, 2024, **43**, 100252.
133 P. Guo, J. Shin, A. G. Greenaway, J. G. Min, J. Su, H. J. Choi, L. Liu, P. A. Cox, S. B. Hong and P. A. Wright, *Nature*, 2015, **524**, 74–78.
134 J. Shin, H. Xu, S. Seo, P. Guo, J. G. Min, J. Cho, P. A. Wright, X. Zou and S. B. Hong, *Angew. Chem., Int. Ed.*, 2016, **55**, 4928–4932.
135 G. Lewis, M. Miller, J. Moscoso, B. Wilson, L. Knight and S. Wilson, *Studies in Surface Science and Catalysis*, Elsevier, 2004, 154, pp. 364–372.
136 A. Chawla, R. Li, R. Jain, R. J. Clark, J. G. Sutjianto, J. C. Palmer and J. D. Rimer, *Mol. Syst. Des. Eng.*, 2018, **3**, 159–170.
137 D. Schwalbe-Koda and R. Gómez-Bombarelli, *AI-Guided Des. Prop. Predict. Zeolites Nanoporous Mater.*, 2023, 81–111.
138 D. C. Elton, Z. Boukouvalas, M. D. Fuge and P. W. Chung, *Mol. Syst. Des. Eng.*, 2019, **4**, 828–849.
139 M. Wu, S. Zhang and J. Ren, *APL Mater.*, 2025, **13**, 020601.
140 G. Sastre and F. Daeyaert, *AI-Guided Design and Property Prediction for Zeolites and Nanoporous Material*, Wiley, 2023.
141 Z. Jensen, E. Kim, S. Kwon, T. Z. Gani, Y. Román-Leshkov, M. Moliner, A. Corma and E. Olivetti, *ACS Cent. Sci.*, 2019, **5**, 892–899.
142 K. Muraoka, Y. Sada, D. Miyazaki, W. Chaikittisilp and T. Okubo, *Nat. Commun.*, 2019, **10**, 4459.
143 X. Peng, R. Pan, X. Li, W. Zhong and F. Qian, *Chem. Eng. Sci.*, 2025, 121378.
144 R. Todeschini and P. Gramatica, *Perspect. Drug Discovery Des.*, 1998, **9**, 355–380.
145 M. Moliner, Y. Román-Leshkov and A. Corma, *Acc. Chem. Res.*, 2019, **52**, 2971–2980.
146 Z. Jensen, S. Kwon, D. Schwalbe-Koda, C. Paris, R. Gómez-Bombarelli, Y. Román-Leshkov, A. Corma, M. Moliner and E. A. Olivetti, *ACS Cent. Sci.*, 2021, **7**, 858–867.
147 P. C. Kotsias, J. Arús-Pous, H. Chen, O. Engkvist, C. Tyrchan and E. J. Bjerrum, *Nat. Mach. Intell.*, 2020, **2**, 254–265.
148 D. Schwalbe-Koda and R. Gómez-Bombarelli, *J. Chem. Phys.*, 2021, **154**, 174109.
149 Organic Structure Database, **https://zeodb.mit.edu/index**, (accessed 18/12/2024).
150 D. Schwalbe-Koda, A. Corma, Y. Román-Leshkov, M. Moliner and R. Gómez-Bombarelli, *J. Phys. Chem. Lett.*, 2021, **12**, 10689–10694.
151 D. Schwalbe-Koda, O. A. Santiago-Reyes, A. Corma, Y. Román-Leshkov, M. Moliner and R. Gómez-Bombarelli, *Chem. Mater.*, 2022, **34**, 5366–5376.
152 E. Pan, S. Kwon, Z. Jensen, M. Xie, R. Gómez-Bombarelli, M. Moliner, Y. Román-Leshkov and E. Olivetti, *ACS Cent. Sci.*, 2024, **10**, 729–743.
153 M. Gálvez-Llompart, A. Cantín, F. Rey and G. Sastre, *Z. Kristallogr. – Cryst. Mater.*, 2019, **234**, 451–460.
154 F. Daeyaert, F. Ye and M. W. Deem, *Proc. Natl. Acad. Sci. U. S. A.*, 2019, **116**, 3413–3418.
155 J. H. Schuur, P. Selzer and J. Gasteiger, *J. Chem. Inf. Comput. Sci.*, 1996, **36**, 334–344.
156 M. Gálvez-Llompart and G. Sastre, *AI-Guided Des. Prop. Predict. Zeolites Nanoporous Mater.*, 2023, 61–80.
157 M. Xie, D. Schwalbe-Koda, Y. M. Semanate-Esquivel, E. Bello-Jurado, A. Hoffman, O. Santiago-Reyes, C. Paris, M. Moliner and R. Gómez-Bombarelli, *ChemRxiv*, 2025, preprint, DOI: **10.26434/chemrxiv-2024-d74sw**.
158 F. Daeyaert and M. Deem, *AI-Guided Des. Prop. Predict. Zeolites Nanoporous Mater.*, 2023, 33–59.
159 D. W. Lewis, D. J. Willock, C. R. A. Catlow, J. M. Thomas and G. J. Hutchings, *Nature*, 1996, **382**, 604–606.

160 (*a*) D. W. Lewis, G. Sankar, J. K. Wyles, J. M. Thomas, C. R. A. Catlow and D. J. Willock, *Angew. Chem., Int. Ed. Engl.*, 1997, **36**, 2675–2677; (*b*) P. Barrett, R. Jones, J. Thomas, G. Sankar, I. Shannon and C. Catlow, *Chem. Commun.*, 1996, 2001–2002.

161 (*a*) R. Pophale, F. Daeyaert and M. W. Deem, *J. Mater. Chem. A*, 2013, **1**, 6750–6760; (*b*) F. Daeyaert and M. W. Deem, *Mol. Inf.*, 2017, **36**, 1600044.

162 F. Daeyaert and M. W. Deem, *J. Mater. Chem. A*, 2019, **7**, 9854–9866.

163 F. Daeyaert and M. W. Deem, *Mol. Phys.*, 2018, **116**, 2836–2855.

164 (*a*) F. Daeyaert and M. W. Deem, *RSC Adv.*, 2019, **9**, 41934–41942; (*b*) F. Daeyaert and M. W. Deem, *ChemPlusChem*, 2020, **85**, 277–284.

165 M. Dorigo, V. Maniezzo and A. Colorni, *IEEE Trans. SMC, Part B*, 1996, **26**, 29–41.

166 K. Muraoka, W. Chaikittisilp and T. Okubo, *Chem. Sci.*, 2020, **11**, 8214–8223.

167 K. T. Butler, D. W. Davies, H. Cartwright, O. Isayev and A. Walsh, *Nature*, 2018, **559**, 547–555.

168 R. Gómez-Bombarelli, J. N. Wei, D. Duvenaud, J. M. Hernández-Lobato, B. Sánchez-Lengeling, D. Sheberla, J. Aguilera-Iparraguirre, T. D. Hirzel, R. P. Adams and A. Aspuru-Guzik, *ACS Cent. Sci.*, 2018, **4**, 268–276.

169 L. Xu, X. Peng, Z. Xi, Z. Yuan and W. Zhong, *Chem. Eng. Sci.*, 2023, **282**, 119188.

170 W. Gao, S. Luo and C. W. Coley, *arXiv*, 2024, preprint, arXiv:2410.03494, DOI: **10.48550/arXiv.2410.03494**.

 